Regulation of neurofilament length and transport by a dynamic cycle of polymer severing and annealing

Atsuko Uchida[1] & Anthony Brown

Department of Neuroscience, Ohio State University, Columbus, OH 43210, USA

[1]Present address:
Department of Biochemistry
Medical College of Wisconsin
Basic Science Building Room 338
8701 Watertown Plank Road
Milwaukee, WI 53226

Address correspondence to:
Dr. Anthony Brown
Department of Neuroscience
Ohio State University
Rightmire Hall
1060 Carmack Road
Columbus, OH 43210
Tel: (614) 292 1205
E-mail: brown.2302@osu.edu

Condensed title: Severing and annealing of neurofilaments

Keywords: neurofilament, axonal transport, severing, annealing, phosphorylation

ORCiD:
Atsuko Uchida http://orcid.org/0000-0002-4658-1504
Anthony Brown http://orcid.org/0000-0003-2295-2929

Title: 87 characters

Abstract length: 160 words

Summary: 37 words

Introduction: 571 words

Discussion: 1886 words

Article length (excluding Methods and References): 39,762 characters

Number of figures: 10

Number of supplementary figures: 3

Number of supplementary tables: 1

Number of supplementary videos: 10

ABSTRACT

We used long-term multi-field time-lapse imaging to analyze the movement, severing and annealing of single neurofilaments along axons of cultured neurons. All filaments were capable of rapid movement. However, long filaments paused and reversed more often, resulting in little net movement, whereas short filaments moved persistently for long distances, pausing and reversing less often. Long filaments severed more frequently, generating shorter filaments, and short filaments annealed more frequently, generating longer filaments. Site-directed mutagenesis to mimic phosphorylation at known phosphorylation sites in the neurofilament protein L head domain increased the severing rate, generating shorter neurofilaments that moved more frequently. A dephospho-mimic mutant had the opposite effect. Treatment with activators of protein kinase A increased filament severing, and this effect was blocked by the dephospho-mimic. Thus, neurofilament length and transport are regulated by a dynamic cycle of severing and annealing. We propose that focal destabilization of intermediate filaments by N-terminal phosphorylation may be a general enzymatic mechanism for severing these cytoskeletal polymers.

SUMMARY

Uchida & Brown demonstrate that neurofilament length and transport are regulated by a dynamic cycle of neurofilament polymer severing and end-to-end annealing and propose an enzymatic severing mechanism for neurofilaments involving N-terminal phosphorylation of their constituent polypeptides.

INTRODUCTION

Neurofilaments, which are the intermediate filaments of nerve cells, are space-filling polymers that accumulate in axons during development to expand axon caliber and thus increase axonal conduction velocity (Hoffman, 1995; Lariviere and Julien, 2004). These polymers are assembled in the neuronal cell body (Black et al., 1986) and transported into and along axons by the mechanisms of axonal transport (Roy et al., 2000; Wang et al., 2000). Notably, neurofilaments are unique among other known axonally transported cargoes in that they are long flexible protein polymers, measuring just 10 nm in diameter and up to 40 μm or more in length (Fenn et al., 2018a; Fenn et al., 2018b; Yan and Brown, 2005). These polymers move bidirectionally along microtubule tracks powered by kinesin and dynein motors (Francis et al., 2005; He et al., 2005; Uchida et al., 2009). The movement is characterized by short bouts of rapid movement interrupted by prolonged pauses, resulting in an overall slow rate of movement (Brown, 2000). Keratin and vimentin filaments have also been reported to move along microtubule tracks, suggesting that such movements are a general property of intermediate filaments (Leduc and Etienne-Manneville, 2017; Robert et al., 2019).

Studies *in vitro* have shown that intermediate filaments lengthen by joining at their ends, a process known as end-to-end annealing (Herrmann et al., 1999; Mucke et al., 2016; Wickert et al., 2005). Using photobleaching/photoconversion strategies, we demonstrated end-to-end annealing of vimentin filaments and neurofilaments in cell lines (Colakoglu and Brown, 2009), and we documented extensive end-to-end annealing of neurofilaments in primary neurons (Uchida et al., 2013). In the course of those studies, we also encountered examples of neurofilament severing (Fenn et al., 2018a; Uchida et al., 2013). Subsequently, severing and annealing of vimentin filaments has also been reported by others (Hookway et al., 2015). End-to-end annealing occurs spontaneously *in vitro* in the absence of accessory factors (Winheim et al., 2011), and likely involves overlap or interdigitation of the staggered coiled coil dimer overhangs at the ends of each intermediate filament (Colakoglu and Brown, 2009; Lopez et al., 2016). However, the mechanism of intermediate filament severing is unknown.

The discovery that neurofilament length can be altered by severing and annealing raises the question of the significance of neurofilament length for neurofilament function. Given that neurofilaments in cultured neurons can be as long as 183 μm in length (Brown, 1997), we reasoned that their length might influence their axonal transport. However, analysis of

neurofilament transport on short time scales (seconds or minutes) has revealed no decrease in neurofilament transport velocity with increasing polymer length for filaments ranging from 0.6-42 μm in length (Fenn et al., 2018a). Here we show that there is actually a strong dependence of neurofilament transport on filament length, but only on longer time scales (tens of minutes). Long and short filaments both exhibit bouts of rapid movement, but long filaments pause and reverse direction more often. This resulted in far less net movement of long filaments on long time scales. In addition, we quantify for the first time the rates of annealing and severing in axons and find that these differ with respect to filament length, with long filaments severing more frequently and short filaments annealing more frequently. Our data suggest that neurofilament length and transport are regulated by a dynamic cycle of severing and annealing. We show that this cycle is regulated by phosphorylation and that site-directed phosphorylation may be a mechanism for neurofilament severing.

METHODS

Molecular cloning

The rat pNFL-myc, pNFL^{S2,55,57,66A}-myc, pNFL^{S2,55,57,66D}-myc, pNFL^{S2A}, pNFL^{S2D}, pNFL^{S55A}, pNFL^{S55D}, pNFL^{S57A}, pNFL^{S57D}, pNFL^{S66A} and pNFL^{S66D} cDNA expression constructs were provided by Chris Miller (Yates et al., 2009). The pNFL-myc, pNFL^{S2,51,55,66A}-myc and pNFL^{S2,55,57,66D}-myc constructs encoded a myc epitope tag linked to the C terminus of rat neurofilament protein L (NFL), whereas the other mutants lacked a myc tag. To make the pNFL-GFP, pNFL^{S2,55,57,66A}-GFP and pNFL^{S2,55,57,66D}-GFP fluorescent fusion constructs, we used polymerase chain reaction (PCR) to replace the myc tag in the pNFL-myc, pNFL^{S2,51,55,66A}-myc, pNFL^{S2,55,57,66D}-myc constructs with GFP by cloning the NFL sequences into a pEGFP-N3 vector (Clontech/Takara Bio) between the EcoR1 and BamH1 restriction sites of the multiple cloning site. The forward and reverse PCR primers were 5'-CGA CTC ACT ATA GGC TAG CCT CGA GAA TTC CTG AGG-3' and 5'-CGC GGA TCC ATC TTT CTT CTT AGC AGC TTG C-3' respectively. The resulting vectors encoded for GFP linked to the C-terminus of rat NFL by a 5 amino acid linker with the sequence -Gly-Ser-Ile-Ala-Thr-. To make the mouse pNFL-GFP fluorescent fusion construct, we first amplified the mouse NFL coding region by PCR using the mouse pNFL-paGFP construct (Uchida et al., 2013) as a template. The forward and reverse PCR primers were 5'-CAT TGA CGC AAA TGG GCG GTA G-3' and 5'-CGG GAT CCA TCT TTC TTA GCC AC-3' respectively. This PCR product was then cloned into the rat pNFL-GFP construct between the NheI and BamH1 sites to replace the rat sequence with the mouse sequence. To make the mouse pNFL^{S2,55,57,66A}-GFP and pNFL^{S2,55,57,66D}-GFP fluorescent fusion constructs, we used custom gene synthesis (GenScript, NJ, USA) to create 361 bp DNA fragments spanning the coding region for the first 99 amino acids at the N-terminus of mouse NFL (with either the S2,55,57,66A or S2,55,57,66D mutations) flanked by XhoI and PvuI restriction sites. We then cloned these fragments between the corresponding XhoI and PvuI restriction sites of the mouse pNFL-GFP construct. The resulting vectors encoded for GFP linked to the C-terminus of mouse NFL by a 5 amino acid linker with the sequence -Gly-Ser-Ile-Ala-Thr-, identical to the linker in the rat constructs. All constructs were confirmed by sequencing the entire open reading frame.

A note about the residue numbering in NFL

Note that there is some inconsistency between the literature and genomic sequence databases concerning the numbering of the phosphorylated serines in the NFL head domain. NFL was first sequenced by Edman degradation, and that reported sequence lacked the N-terminal methionine

and thus started with a serine (Geisler et al., 1985). This was subsequently confirmed by others using mass spectrometry, and the N-terminal serine was found to be acetylated (Betts et al., 1997; Cleverley et al., 1998; Trimpin et al., 2004), which suggests that the N-terminal methionine of NFL is removed post-translationally. Thus, the serines in the NFL head domain are consistently numbered in the literature starting from the second amino acid residue (serine) in the NFL open reading frame (e.g.Giasson et al., 1996; Hashimoto et al., 2000; Nakamura et al., 2000; Yates et al., 2009). In contrast, NFL residues that are mutated in human disease (e.g. mutations in NFL which cause Charcot-Marie-Tooth disease) are numbered assuming methionine is the first residue. While the widely accepted convention is to number amino acids based on the primary translation product, with methionine being residue 1, we number them from the second residue in this article in order to maintain consistency with the extensive literature on NFL phosphorylation. Specifically, the serines mutated in the present study are actually in positions 3, 56, 58 and 67 of the predicted primary translation product, but are referred to in this article as serines 2, 55, 57 and 66.

NFL knockout mice

$NFL^{+/-}$ heterozygous mice (Zhu et al., 1997) were obtained from Don Cleveland at UCSD and maintained heterozygous in our facility by crossing with wild type C57BL/6 mice. To maintain this mouse colony, heterozygotes were crossed and $NFL^{-/-}$ homozygotes ("knockouts") were obtained in the expected Mendelian proportions. Genotyping was performed by PCR using tail DNA with the forward primer 5'-GCT ATT CGG CTA TGA CTG GGC ACA A-3' and the reverse primer 5'-CGA TGT TTC GCT TGG TGG TCG AAT G -3' for detecting the Neo cassette. The size of the amplified product was 366 bp. The forward primer, 5'-GCA ACG ACC TCA AGT CTA TCC GCA-3' and reverse primer, 5'-CTT CGG CGT TCT GCA TGT TCT TGG -3' were used for detecting the wild type allele. The size of the amplified product was 597 bp.

Cell culture and transfection

Cortical neurons from mice and rats were cultured using the glial sandwich technique of Kaech and Banker (2006) with the modifications described by Uchida et al. (2016). We used rat glia for both rat and mouse neuronal cultures. To prepare glial cultures, the cerebral cortices of 4 to 6 P0 rats were dissociated and chopped in Ca^{++}/Mg^{++}-free Hank's Balanced Salt Solution (HBSS; Invitrogen, Carlsbad, CA). The tissue pieces were dissociated in PBS containing 0.25% [w/v] trypsin (Worthington Biochemical Corp., Lakewood, NJ), 1% [w/v] DNase-I (Sigma, St. Louis, MO) and 0.27mM EDTA (Sigma). The resulting cell suspension was plated in a $75cm^3$ flask and

maintained at 37°C in glial medium consisting of Minimum Essential Medium (Invitrogen) supplemented with 10% [v/v] horse serum (Invitrogen), 0.7% [w/v] glucose (Sigma) and 5 µg/ml gentamicin (Invitrogen), in an atmosphere of 5% CO_2. After 2 hr, the flask was swirled to remove loosely attached cells and then fed with fresh glial medium. The cells were typically passaged just once onto poly-D lysine (Sigma) coated coverslips about two days before the intended day of use. The glial medium was replaced with neuronal plating medium (see below) on the day of use.

To prepare neuronal cultures, the cerebral cortex of one P0 mouse was dissociated in PBS containing 0.025% [w/v] Trypsin, 0.27mM EDTA (Sigma) and 0.5% [w/v] DNase-I for each transfection. The dissociated cortical neurons were transfected by electroporation prior to plating using an Amaxa Nucleofector™ (Lonza Inc., Walkersville, MD) with the rat neuron Nucleofection kit (VPG-1003) and program G013. The volume of the cell suspension was 100 µl and the cell density ranged from 4-6 × 10^6 cells/ml. The DNA consisted of a mixture of 5 µg pNFL-GFP construct, 5 µg pNFM construct and 5 µg EB3-mCherry construct. We used rat constructs when transfecting rat neurons and mouse constructs when transfecting mouse neurons. The cells were then plated onto glass-bottomed dishes that had been coated with poly-D-lysine. Glass coverslips bearing glia (>80% confluency) were suspended over the neurons using dots of paraffin wax as spacers. The resulting sandwich cultures were maintained initially at 37ºC/5% CO_2 in neuronal plating medium, which consisted of NbActiv4 (BrainBits; Brewer et al., 2008) supplemented with 5% [v/v] fetal bovine serum (FBS; Thermo Scientific) and 5 µg/ml gentamicin. On the day after plating, this medium was replaced with neuronal culturing medium. The neuronal culturing medium was identical to the plating medium except that it lacked serum and also contained 5 µM cytosine arabinoside (AraC; Sigma). Every two days, half the medium was removed and replaced with fresh medium.

Human adrenal adenocarcinoma SW13vim- cells, which lack endogenous vimentin (Sarria et al., 1990), were cultured in DMEM/F12 medium (Thermo Fisher Scientific) supplemented with 5% fetal bovine serum (HyClone, GE Healthcare, Chicago, IL) and 10 µg/ml gentamicin (MilliporeSigma, Burlington, MA). These cells were transfected with Lipofectamine 2000 (Thermo Fisher Scientific) as described previously (Colakoglu and Brown, 2009; Stone et al., 2019).

Protein kinase A activation

8-bromo cAMP and/or okadaic acid were added directly to the culture medium at final concentrations of 2 mM and 5 nM, respectively, and mixed gently with a pipette. For 8-bromo-

cAMP, we incubated the cultures for 5 hr prior to imaging. For okadaic acid, we incubated the cultures for 2 hr prior to imaging. For combined treatment with both reagents, we first added 8-bromo cAMP, incubated for 3 hr, and then added okadaic acid. After incubation for an additional 2 hr, the cells were kept in the medium containing the two reagents and imaged for up to 5 hr.

Microscopy and imaging

For imaging, the neuronal cell culture medium was replaced with Hibernate-A medium (BrainBits, low fluorescence formulation) with 2% (v/v) B27 supplement mixture, 0.5 mM Glutamax (Invitrogen) and 37.5 mM NaCl to increase the osmolarity to ~310-320 mOs. To maintain the temperature at 37°C, we used a stage-top incubator with a humidity module (Okolab, Ottaviano, NA, Italy) and an objective heater (Bioptechs, Butler, PA). The cells were observed with a Nikon TiE inverted wide-field epifluorescence microscope equipped with a 100x/1.4NA Plan-Apochromat VC oil immersion objective, SOLA LED light source (Lumencor, Beaverton, OR), and Nikon TI-S-ER motorized stage with X-Y linear encoders. The exciting light was attenuated to 10-15% transmission using the LED light source controller. Images were acquired with no pixel binning using an Andor iXon Ultra 897 electron multiplying cooled CCD (EMCCD) camera (Andor Technology, Belfast, UK), which has a 512 x 512 array of 16 x 16 μm pixels, and MetaMorph™ software (Molecular Devices, Sunnyvale, CA). The GFP and mCherry fluorescence was imaged using an ET-GFP filter cube (model 49002, Chroma Technology, Brattleboro, VT) or an ET-mCherry/Texas Red filter cube (model 49008; Chroma). The movement of GFP-tagged neurofilaments was recorded by acquiring time-lapse movies for a duration of 15 or 30 minutes using 100 ms exposures and 3 s time intervals. For our analyses of the frequency of neurofilament movement, the movies were acquired at a fixed location, which we refer to as fixed-field time-lapse movies. For our analyses of the long-term kinetic behavior of single neurofilaments, we acquired multi-field time-lapse movies by moving the field of view during the acquisition (described below). The movement of EB3-mCherry comets was recorded by acquiring fixed-field time-lapse movies for a duration of 5 minutes using 1 s exposures and 3-5 s time intervals.

Multi-field tracking

To analyze the long-range motile behavior of single filaments, we developed a multi-field time-lapse tracking method to follow the movement of filaments over distances that exceed the field of view of our camera (Uchida et al., 2016). This method takes advantage of the motorized stage on our microscope and the “Move stage to image position” function in the MetaMorph™ software

("Offset stage position with mouse click" and "Move stage immediately on mouse click" options selected) to re-center the filament whenever it approaches the edge of the camera field of view. First, we selected an isolated filament to track by observing the acquired images live during time-lapse image acquisition. When the selected filament approached the edge of the camera field of view, we clicked on it. This caused the stage to move automatically to center that position (and thus the filament being tracked) within the field of view. By repeating this process, it was possible to track single filaments along axons over distances of 1 mm or more. Our time-lapse interval of 3 s was sufficient time to allow the mouse to be clicked, the stage to move, and the new stage position to register before the next image is acquired, thereby allowing continuous time-lapse acquisition of the moving filament. We aimed to follow each filament for 30 min, but we terminated the movie acquisition earlier than that if the filament reached the end of the axon, entered either the cell body or growth cone, or was lost due to overlap with other filaments. To confirm axon orientation, we acquired a fixed-field time-lapse movie of the EB3-mCherry fluorescence before or after the multi-field time-lapse movie and tracked the direction of movement of EB3 comets, which corresponds to the anterograde direction (Fenn et al., 2018a). Axons with ambiguous directionality were excluded from our analysis.

To track neurofilament movement in the multi-field time-lapse movies, the image planes were stitched together using the x-y coordinates of the stage (saved in the image header) to create a multi-field montage from the movie planes. Briefly, a blank image stack was created with x and y dimensions large enough to span the total distance travelled by the tracked filament. Each image frame was then copied into the corresponding frame of the new stack, thus shifting the image position to account for the stage movement. When the resulting movie is played back, the camera field appears to skip across the field following the moving filament. The x-y coordinates of one end of the filament were then recorded in successive movie frames using the "TrackPoints" option in the Motion analysis drop-in of the MetaMorph™ software. To be consistent, for each filament we selected the end that was leading when the filament was moving in its net direction of movement and tracked that same end throughout the movie. The coordinates and other parameters such as elapsed time, direction, and velocity were logged to a Microsoft Excel spreadsheet via Dynamic Data Exchange for further analysis.

Analysis of neurofilament movement, severing and annealing

For the multi-field time-lapse movies, all filaments greater than or equal to 10 pixels (1.6 μm) in length were analyzed if they moved a total distance of at least 50 pixels (8 μm). Since severing

and annealing resulted in a change in filament length, we excluded daughter filaments resulting from annealing or severing events from our analysis. The net velocity was calculated by dividing the net distance moved by each filament during the course of each movie by the elapsed time. Since neurofilaments can exhibit frequent folding behaviors while they are pausing but are almost always fully extended when they move (Fenn et al., 2018b), we only measured filament length during bouts of movement. To avoid motion blurring, we measured the filaments during brief pauses rather than during bouts of rapid movement. To quantify annealing frequency, we only counted events in which the adjoined filaments moved together as one after the putative annealing event. We measured the filaments before and after the putative annealing event to ensure conservation of length. To quantify severing frequency, we only counted events in which the filaments moved before breaking (in order to be sure that it was indeed a single filament) and in which there was clear separation between the resulting fragments (e.g. due to movement of one or both of the fragments). To quantify the frequency of neurofilament movement in fixed-field time-lapse movies, we located the midpoint of the longest gap in the neurofilament array in the field of view and drew a line perpendicular to the axon at that location. We then counted the number of filaments that moved across each line during the course of that movie. If there were multiple gaps along a single axon, we selected the longest for our analysis; we did not analyze more than one gap per axon.

Immunofluorescence microscopy

Neurons were fixed with 4% formaldehyde and then extracted with PBS containing 1% [v/v] Triton X-100 and 0.3 M NaCl. After fixation and extraction, the cells were first immunostained with a mouse monoclonal specific for phospho-independent NFM (RMO270; Invitrogen, 1:400) and subsequently with a rabbit polyclonal antibody specific for myc tag protein (71D10: Cell Signaling, 1:100). The secondary antibodies were Alexa 488-goat anti-mouse (Invitrogen, 1:200) and Alexa 568-goat anti-rabbit (Invitrogen, 1:200). Coverslips were mounted using ProLong Gold Antifade reagent (Invitrogen). Images were acquired on an Andor Revolution WD spinning disk confocal, which incorporates a Yokogawa CSU-W1 confocal scanning unit attached to a Nikon TiE inverted microscope with a 100x Plan Apo 1.0 NA oil immersion objective and an Andor iXon Ultra 897 EMCCD camera. SW13vim- cells were fixed with 4% formaldehyde in PBS and immunostained as described above. Images were acquired on the same microscope but using an Andor Neo sCMOS camera.

Statistical analysis

Statistical analysis was performed using SPSS software (IBM, Armonk, NY). Tests for deviations from normality were performed using the Shapiro-Wilk test. Tests comparing normally distributed data were performed using a t-test. Tests for homogeneity of variance, which is an assumption of the t-test, were performed using Levene's test. Tests comparing non-normally distributed data were performed using the Mann-Whitney-Wilcoxon test.

RESULTS

To visualize neurofilaments, we co-transfected dissociated cortical neurons with GFP-tagged NFM (GFP-NFM) (Wang and Brown, 2001) and EB3-mCherry (to allow assessment of axon orientation). We then observed the cells after 8-10 days in culture. The GFP fusion protein co-assembles fully with endogenous neurofilament proteins and the low neurofilament content of these neurons makes it possible to track moving filaments for long distances (Uchida et al., 2016). Our previous time-lapse imaging of neurofilament transport was limited to short-term observations because the filaments moved rapidly out of the camera field of view. To overcome this problem, we watched the moving filaments continuously during time-lapse image acquisition and used the motorized stage on our microscope to re-center them when they approached the edge of the field of view. We then used the recorded stage position of each frame in the resulting movies to register the images, creating a movie montage (Movie S1), and tracked the movement of the filaments manually in these movie montages using the TrackPoints™ tools in the MetaMorph™ software (Fig. 1). Using this multi-field time-lapse tracking approach, we were able to follow the movement of single neurofilaments along axons for distances of 1 mm or more.

Dependence of transport kinetics on filament length

To investigate the dependence of neurofilament transport on polymer length, we acquired 76 long-term time-lapse movies of moving filaments in neonatal rat cortical neurons after 8-10 days in culture. The resulting movies often also captured the movement of other filaments. Thus, during the subsequent analysis, we tracked all filaments in the movies that met our analysis criteria (see Methods). In total, we obtained trajectories for the movement of 93 filaments, which ranged from 1.3 to 48.3 μm in length. Fifty-five moved in a net anterograde direction and 38 moved in a net retrograde direction.

Fig. 2 shows representative examples of the trajectories of eight filaments, four “short” filaments (2.5-6.9 μm in length) and four “long” filaments (18.9-31.3 μm in length). As we have reported previously, on short time scales (seconds to minutes), both short and long filaments moved rapidly (Fenn et al., 2018a). However, on longer time scales (tens of minutes), we observed a marked difference. Short filaments exhibited a clear directional preference (anterograde or retrograde), and they tended to move persistently in that direction throughout the tracking period, pausing and reversing relatively infrequently (Fig. 2A-D). Long filaments were capable of rapid movement, sometimes for several minutes or more, but they also paused for more prolonged periods and

reversed direction more frequently. As a result, the movement of long filaments often resulted in little net displacement (Fig. 2E-H).

Fig. 3A shows a scatter plot of net average transport velocity versus filament length for all 93 filaments that we tracked, and Fig. 3G shows a histogram of this data. Figs. 3C & E show scatter plots of the corresponding tracking durations and distances for those filaments. Each point in the scatter plots represents the data for one filament. On average there was a trend towards lower net velocities for longer filaments, which became more pronounced if we excluded 28 filaments in this data set that were tracked for less than 8 min (Fig. 3B,D,F & H). For short filaments (<10 μm) that were tracked for at least 8 min, the net average velocity was 0.47 μm/s anterograde and 0.86 μm/s retrograde, but as filament length increased, this average velocity decreased (Fig. 3H). For longer filaments (>20 μm), net average velocities of 0.11 μm/s anterograde and 0.18 μm/s retrograde indicated much less movement. Quantification of the moving and pausing behavior confirmed that this decrease in net average velocity was due to an increase in the time that the filaments spent pausing from 37% to 62% (Fig. 4A) and a decrease in their directional persistence, i.e. the proportion of the time the filaments spent moving in the direction of their net movement, from 85% to 43% (Fig. 4B). In contrast, though there was considerable scatter in the data, the absolute peak velocity exhibited no clear length-dependence (Fig. 4C).

Dependence of annealing and severing frequency on filament length

As mentioned above, the filaments that we tracked sometimes exhibited severing or end-to-end annealing. Examples are shown in Fig. 5 and Movies S2 and S3. To quantify annealing and severing frequency, we counted the total number of annealing and severing events in the 76 movies analyzed above. We also included an additional 21 movies that we excluded from the original data set due to ambiguity in the axon orientation or due to the use of time-lapse intervals of 2 s instead of 3 s. In total, we observed 32 severing events and 16 end-to-end annealing events, corresponding to an average severing rate of 1.0/hr and an average annealing rate of 0.5/hr (141 filaments tracked; 32 hr total tracking time). To investigate the effect of filament length, we analyzed the dependence of these rates on the length of the tracked filament (Fig. 5C,D). Short filaments (<10 μm) exhibited the highest rate of end-to-end annealing (1.23 events/hr) but the lowest rate of severing (0.34 events/hr). In contrast, long filaments (>20 μm) exhibited the lowest rate of annealing (0.15 events/hr) and the highest rate of severing (1.5 events/hr). Filaments of intermediate length (10-20 μm) exhibited intermediate rates of severing and

annealing. Thus, the rates of severing and end-to-end annealing exhibit inverse length dependencies.

Phospho- and dephospho-mimics of NFL have different effects on neurofilament length, transport, severing and annealing

It is known that the intermediate filament protein head domains regulate filament assembly (Gill et al., 1990), and phosphorylation of these domains induces intermediate filament fragmentation and disassembly *in vitro* and *in vivo* in a variety of cell types (Ando et al., 1989; Chou et al., 1996; Eriksson et al., 2004; Hisanaga et al., 1990; Inagaki et al., 1987; Izawa and Inagaki, 2006; Klymkowsky et al., 1991). Thus, phosphorylation of the N-terminal head domains of the neurofilament subunit proteins at loci along neurofilament polymers could be a mechanism for neurofilament severing. To test this hypothesis, we obtained a panel of rat NFL constructs from Chris Miller (King's College, University of London) in which the four serines in the NFL head domain that have been proposed to be phosphorylated in neurons (serines 2, 55, 57, 62) were mutated to either aspartate or alanine (Yates et al., 2009). Serines 2, 55 and 62 have been reported to be phosphorylated by protein kinase A (Cleverley et al., 1998; Giasson et al., 1996; Nakamura et al., 2000; Sihag and Nixon, 1991; Trimpin et al., 2004), and serine 57 by Rho Kinase and calcium-calmodulin dependent kinase (CaMKII) (Hashimoto et al., 1998; Hashimoto et al., 2000). Both the $NFL^{S2,55,57,66A}$ (dephospho-mimic) and $NFL^{S2,55,57,66D}$ (phospho-mimic) mutants co-assembled with NFM in SW13vim- cells (Fig. S1).

To investigate the effect of NFL phosphorylation on neurofilaments in neurons, we expressed fluorescent fusions of wild type, dephospho-mimic or phospho-mimic NFL (NFL-GFP, $NFL^{S2,55,57,66A}$-GFP or $NFL^{S2,55,57,66D}$-GFP, respectively) in cultured neonatal rat cortical neurons. In comparison to GFP-NFM, we found that transfection with NFL-GFP alone tended to result in more cells with elevated diffuse fluorescence, which obscured the gaps in the neurofilament array. To address this problem, and thus yield more cells suitable for imaging, we co-transfected the NFL-GFP fusions with untagged NFM. Under these conditions, both the $NFL^{S2,55,57,66A}$-GFP and $NFL^{S2,55,57,66D}$-GFPNFL constructs incorporated fully into neurofilament polymers throughout the cells with no little or no detectable diffuse fluorescence (Fig. 6). In contrast to Yates et al. (2009), we did not observe any tendency for the $NFL^{S2,55,57,66D}$ mutant to aggregate.

First, we investigated the neurofilament length distribution and transport frequency in fixed-field time-lapse movies of neurons expressing wild type NFL-GFP. The average filament length

increased with age in culture from 6.2 μm at 8 days to 9.2 μm at 11 days, and the average frequency decreased from 7.9 filaments/axon/hr at 8 days to 2.3 filaments/axon/hr at 11 days (Table S1). Thus, neurofilaments become longer and less mobile as these neurons mature. To investigate the effect of the phospho- and dephospho-mimics, we focused on neurons after 8 days in culture (Fig. 7). The average length of filaments containing wild type NFL-GFP at this age was 6.3 μm (Fig. 7B). Filaments containing the phospho-mimic $NFL^{S2,55,57,66D}$-GFP were shorter (average length=5.1 μm; Fig. 7C), whereas filaments containing the dephospho-mimic $NFL^{S2,55,57,66A}$-GFP were longer (average length=13.5 μm; Fig. 7A). Filaments containing wild type NFL-GFP moved with an average frequency of 7.9 neurofilaments/axon/hr (Fig. 7E). Filaments containing the phospho-mimic $NFL^{S2,55,57,66D}$-GFP moved slightly more frequently (8.2 neurofilaments/axon/hr; Fig. 7D), whereas filaments containing the dephospho-mimic $NFL^{S2,55,57,66A}$-GFP moved less frequently (3.1 neurofilaments/axon/hr; Fig. 7F). Interestingly, we also observed that in older cultures (after 16-21 days in culture), the neurofilament content was higher in axons expressing the dephospho-mimic $NFL^{S2,55,57,66A}$-GFP than in axons expressing the phospho-mimic $NFL^{S2,55,57,66D}$-GFP (Fig. S2). Thus, phosphorylation of these sites regulates neurofilament length, which in turn regulates neurofilament transport and accumulation during axonal maturation.

To investigate the mechanism by which NFL phosphorylation influences neurofilament length, we acquired multi-field time-lapse movies and quantified the frequency of neurofilament severing and annealing. The severing frequency of filaments containing the dephospho-mimic $NFL^{S2,55,57,66A}$ mutant was uniformly low (<0.4 events/hr) for all filament lengths (Fig. 8C), whereas the severing frequency for filaments containing the phospho-mimic $NFL^{S2,55,57,66D}$ was uniformly high (>1.1 events/hr) for all filament lengths (Fig. 8D). The picture was a little more complex for the annealing frequencies. Short filaments (0-10 μm) containing the dephospho-mimic $NFL^{S2,55,57,66A}$ mutant exhibited the highest annealing frequency that we have observed (2 events/hr). However, this declined with increasing filament length (Fig. 8A), similar to the length-dependence reported above for filaments containing GFP-NFM (Fig. 5C). In comparison, filaments containing the $NFL^{S2,55,57,66D}$ mutant exhibited lower annealing frequencies (1 event/hr) for filaments 0-10 μm in length, higher frequencies (1.3 events/hr) for filaments 10-20 μm in length, and much lower frequencies (0.3 events/hr) for filaments <20 μm in length (Fig. 8B). This length-dependence of the annealing frequencies may be due to the fact that annealing requires an encounter between two filament ends. End-to-end annealing is thus dependent on the frequency of movement (which is in turn length-dependent) in addition to the phosphorylation state of the subunit proteins (see

Discussion). Nevertheless, broadly speaking these data are consistent with the hypothesis that NFL phosphorylation favors severing and dephosphorylation favors annealing.

In principle, the differences between the transport of neurofilaments containing the $NFL^{S2,55,57,66A}$-GFP and $NFL^{S2,55,57,66D}$-GFP mutants could be due to different effects on the structure, chemistry, or interactions of the filaments or because of differences in filament length. To test this, we compared the net velocity of filaments containing these mutant proteins. In keeping with our analysis above, we focused on the long-term kinetic behavior by analyzing only filaments that were tracked for at least 8 min. The dependence of net velocity on filament length was similar for the two mutants (Fig. 8E,F) and also similar to that observed for filaments containing GFP-tagged NFM in Fig. 3H. Short filaments (0-10 μm in length) moved with a higher average net velocity than long filaments (>20 μm in length). This was the case for filaments moving in both net anterograde and net retrograde directions. Thus, the different effects of the phospho- and dephospho-mimic NFL mutants on neurofilament transport were due at least primarily to their effect on neurofilament length.

Activators of protein kinase A reduce neurofilament length

Three of the four sites mutated in the phospho-mimic and dephospho-mimic NFL constructs used above are substrates for protein kinase A (PKA) (Cleverley et al., 1998; Giasson et al., 1996; Giasson and Mushynski, 1998; Hisanaga et al., 1994; Nakamura et al., 2000; Sihag et al., 2007; Sihag and Nixon, 1990; Sihag and Nixon, 1991). Phosphorylation by PKA *in vitro* causes local thinning and fragmentation of NFL homopolymers and native neurofilaments at sites along their length (Hisanaga et al., 1994), and also arrests the assembly NFL homopolymers at the octamer stage (Hisanaga et al., 1990). The neurofilament head domains can also be dephosphorylated by protein phosphatases 1 and 2A (PP1 and PP2A, respectively) (Sacher et al., 1994; Strack et al., 1997). Protein phosphatase 2A (PP2A) dephosphorylates neurofilament proteins that have been phosphorylated by PKA and renders them competent to assemble (Giasson et al., 1996; Saito et al., 1995). Okadaic acid, which is a selective inhibitor of PP1 and PP2A, increases neurofilament head domain phosphorylation and induces reversible neurofilament fragmentation and disassembly in cultured neurons (Giasson et al., 1996; Giasson and Mushynski, 1998; Sacher et al., 1992; Sacher et al., 1994). This effect is thought to be due primarily to PP2A inhibition (Sacher et al., 1994) and is potentiated by PKA activation (Giasson et al., 1996). Collectively, these findings demonstrate that the structural integrity of neurofilaments is regulated by phosphorylation and dephosphorylation of the neurofilament protein head domains, particularly by the antagonistic

effects of PKA and PP2A. Thus, we hypothesized that phosphorylation by PKA is a potential mechanism for neurofilament severing in axons.

To test whether PKA regulates neurofilament length in neurons, we treated cultured neonatal rat cortical neurons expressing wild type, phospho-mimic $NFL^{S2,55,57,66D}$-GFP or dephospho-mimic $NFL^{S2,55,57,66A}$-GFP with 2 mM 8-bromoadenosine 3',5'-cyclic monophosphate (8-Br-cAMP), which is a membrane-permeant activator of PKA, and/or 5 nM okadaic acid after 9 days in culture. We then measured the lengths of moving neurofilaments in time-lapse movies as described above (Fig. S3). The average filament length was 10.7 μm in untreated neurons expressing NFL-GFP. 8-Br-cAMP or okadaic acid alone reduced this average length to 9.1 μm and 8.1 μm respectively, whereas the two together reduced the average length to 5.0 μm. To test if this effect was due to a direct action on neurofilaments, we repeated these experiments with neurons expressing $NFL^{S2,55,57,66A}$-GFP, which is not phosphorylatable at these four sites. The average filament length was 12.9 μm in untreated neurons expressing $NFL^{S2,55,57,66A}$-GFP. 8-Br-cAMP or okadaic acid alone reduced the average length to 10.4 μm and 12.6 μm respectively. The two together reduced the average length to 8.2 μm. Thus, transfection of the neurons with dephospho-mimic $NFL^{S2,55,57,66A}$-GFP partially protected the neurofilaments from the effects of PKA activation.

The above effect was statistically significant, but more modest than we were expecting. A likely explanation for this is that the cells expressed endogenous phosphorylatable NFL in addition to the exogenous mutant NFL. To address this, we repeated the experiment in cortical neurons from neonatal $NFL^{-/-}$ knockout mice using mouse constructs of NFL-GFP and $NFL^{S2,55,57,66A}$-GFP (Fig. 9). As predicted, the effect was much more pronounced. Treatment of cortical neurons expressing NFL-GFP with 8-Br-cAMP plus okadaic acid reduced the average filament length from 9.3 μm to 3.6 μm (Fig. 9A,C). In contrast, the same treatment of cortical neurons expressing $NFL^{S2,55,57,66A}$-GFP, which is not phosphorylatable at these four sites, resulted in only a slight reduction in neurofilament length from 11.8 μm to 11.0 μm (Fig. 9B,D). Thus, the dephospho-mimic $NFL^{S2,55,57,66A}$-GFP almost completely protected the neurofilaments from the effects of PKA activation. These data indicate that the effect of protein kinase activators on neurofilament length was dependent on phosphorylation of NFL and that the kinase acts on one or more of the four sites mutated in the $NFL^{S2,55,57,66A}$-GFP construct.

DISCUSSION

We have used live-cell imaging to investigate the dynamics of neurofilament severing and end-to-end annealing in cultured neurons. Our data establish that severing and annealing are robust and quantifiable features of neurofilament dynamics in neurons. For example, in our experiment on neurons expressing GFP-tagged NFM, we tracked 141 neurofilaments in 97 time-lapse movies (average tracking duration=13.6 min) and recorded 32 incidences of neurofilament severing and 16 instances of end-to-end annealing. Thus, approximately one third of the filaments that we tracked exhibited a severing or annealing event, with an average severing rate of 1.0/hr and an average annealing rate of 0.5/hr.

Since neurofilament severing and annealing alter neurofilament length, we asked what significance the length of these polymers might have. Neurofilaments of all lengths were capable of bouts of rapid movement on short time scales (seconds), as we have reported previously (Fenn et al., 2018a). However, multi-field tracking revealed a difference on long time scales. Short filaments (<10 μm in length) moved rapidly and persistently at average rates of >0.25μm/s for tens of minutes. In contrast, in spite of occasional rapid anterograde and retrograde excursions on short time scales of seconds to minutes, the longest filaments (>30 μm in length) paused and reversed more often. This resulted in little net movement on time scales of many minutes. Thus, polymer length has a profound influence on the transport behavior of neurofilaments.

The mechanism of this length-dependence of the neurofilament movement is unclear. One possibility is that the number of motors recruited by the filaments is low and proportional to their length. If short polymers (<10 μm in length) recruit on average one motor, then these filaments will tend to move persistently for long distances, as we observed, with the direction determined by the type of motor bound. If longer filaments recruit on average multiple motors, then there would be a possibility that they might recruit motors of opposite directionality. This could result in a sort of dynamic tug-of-war in which the filaments might stall for prolonged periods or shuttle between alternating bouts of anterograde and retrograde movement (Fenn et al., 2018a). Presently, this explanation is speculative because we do not know how many motors are required to move neurofilaments, how they attach, or where they attach along the length of these polymers. Such questions are a priority for future studies.

Our data also reveal a novel and intriguing dependency of filament severing and annealing on neurofilament length. Severing creates shorter filaments which move more persistently, pausing and reversing less often. On the other hand, annealing creates longer filaments which pause and reverse direction more often, and thus move less persistently. Long filaments sever more frequently and anneal less frequently, whereas short filaments sever less frequently and anneal more frequently. Thus, neurofilaments undergo a dynamic cycle of severing and end-to-end annealing in axons that regulates neurofilament length and transport kinetics (Fig. 10A).

According to this model, neurofilament length is determined by the balance of the annealing and severing rates. If annealing exceeds severing, filaments will tend to lengthen over time. If severing exceeds annealing, they will tend to shorten. At steady state, as may be achieved in mature non-growing axons, the two rates would be balanced. In our present study, we found that maturation of the neurons in our cultures was accompanied by an increase in the average neurofilament length over time. Thus, we expected to observe more annealing than severing. However, we observed about twice as many severing events as annealing events in our time-lapse movies. While it is possible that this snapshot after 8 days in culture does not reflect the overall dynamics over time, there is also a possible technical explanation for this. Specifically, we can only detect annealing and severing by live-cell imaging in regions of low neurofilament density. Annealing requires an encounter between two filament ends, and thus may be less likely to occur when a filament is isolated than in regions of higher density. In contrast, severing does not require a diffusional encounter between filaments and thus may be independent of filament density. Thus, our method of analysis may tend to favor the detection of severing events over annealing events, leading to an underestimate of the rate of annealing.

An intriguing question is why severing and annealing are dependent on neurofilament length. It is possible that long filaments anneal less frequently simply because they are less mobile and thus collide less frequently. It is also possible that long filaments sever more frequently simply because longer polymers have more potential severing sites. For example, if a severing mechanism tends to target filaments randomly with an average of one severing event per 50 μm polymer per hr, then filaments of this length will tend to sever at an average rate of once per hr whereas filaments that are 5 μm in length will tend to sever at an average rate of 0.1 times per hr. However, we do not rule out the possibility that other mechanisms may apply, such as differential post-translational modification of long and short filaments, or differential interaction of long and short filaments with other cytoplasmic components.

To investigate the effect of phosphorylation on neurofilament length and transport, we used site-directed mutagenesis. Expression of the phospho-mimic mutant ($NFL^{S2,55,57,66D}$) resulted in shorter neurofilaments that moved and severed more frequently, whereas the non-phosphorylatable mutant ($NFL^{S2,55,57,66A}$) had the opposite effect. Remarkably, filaments containing the non-phosphorylatable mutant reached lengths of up to 96 µm, which is the longest moving filament we have ever encountered by live imaging of neurons expressing neurofilament proteins. Treatment with activators of protein kinase A, which has been reported to phosphorylate serines 2, 55 and 62 of NFL, reduced neurofilament length. This effect was blocked by the non-phosphorylatable mutant. These observations suggest that N-terminal phosphorylation of the NFL protein could be a mechanism for neurofilament severing. Specifically, phosphorylation of the head domains of NFL proteins at discrete sites along neurofilaments could locally destabilize these polymers at those sites, leading to filament severing. Since head domain phosphorylation by PKA also induces disassembly of vimentin and keratin filaments (Ando et al., 1989; Ando et al., 1996; Eriksson et al., 2004; Evans, 1988; Inagaki et al., 1987), focal destabilization of intermediate filaments by N-terminal phosphorylation of their constituent polypeptides at specific locations along their length may be a general mechanism for severing this class of cytoskeletal polymers. In this way, phosphorylation at discrete sites along intermediate filaments may represent another tool in the toolbox that cells can use to regulate the organization and dynamics of this class of cytoskeletal polymers.

Since neurofilaments contain about 32 polypeptides per cross-section (Heins et al., 1993), severing likely requires the phosphorylation of multiple subunit proteins at the same location along the polymer, with each additional phosphorylated subunit further weakening the filament at that location and increasing the severing probability (Fig. 10B). While the phosphorylation could be random, it is more likely to occur locally downstream of local signaling events that may be spatially or temporally controlled to locally regulate neurofilament length and transport. Once weakened, the filament could break spontaneously or when pulled on by a motor. In this regard, we have noted that severing often appears to occur at the point at which a filament begins to move. While this may simply reflect the fact that severing can only be confirmed when one fragment moves apart from the other, it is also possible that a weakened filament might break sooner if it is pulled on.

Consistent with this severing model, filaments containing the dephospho-mimic exhibited low rates of severing for all filament lengths, while filaments containing the phospho-mimic exhibited high rates of severing for all filament lengths. However, the effects on filament annealing were more complex. Short filaments containing the dephospho-mimic exhibited higher rates of end-to-end annealing than short filaments containing the phospho-mimic, as expected. In contrast, long filaments containing either mutant exhibited low rates of annealing. Thus, while the severing rates of the filaments containing the phospho- and dephospho-mimic NFL were largely independent of length, the annealing rates retained some length-dependence. This may be due to the lower frequency of movement of long neurofilaments and thus a lower incidence of end-to-end collisions. In contrast, severing is likely to be independent of filament concentration and motility, and thus may be determined solely by subunit phosphorylation.

We focused on PKA in this study because it has been reported to phosphorylate three of the sites mutated in our phospho- and dephospho-mimic NFL constructs. However, we do not exclude the possible involvement of other kinases and/or neurofilament subunits. PKA can phosphorylate the head domains of peripherin, NFM and NFH in addition to NFL (Cleverley et al., 1998; Giasson and Mushynski, 1998; Hisanaga et al., 1994; Huc et al., 1989; Sihag et al., 1999). The NFL head domains can also be phosphorylated by protein kinase C (PKC), Rho kinase, protein kinase N (PKN), and CaMKII (Gonda et al., 1990; Hashimoto et al., 1998; Hashimoto et al., 2000; Hisanaga et al., 1994; Mukai et al., 1996; Nakamura et al., 2000; Sihag et al., 2007; Sihag and Nixon, 1991). PKC has also been reported to phosphorylate NFM and NFH (Sihag et al., 1988) and has been shown to induce intermediate filament disassembly *in vitro* and in cultured cells (Giasson et al., 1996; Hisanaga et al., 1990; Hisanaga et al., 1994). However, our data indicate that treatment with cAMP and okadaic acid is sufficient to induce neurofilament severing, and this can be rescued by expression of the non-phosphorylatable NFL mutant in NFL knockout neurons. Thus, PKA phosphorylation appears to be sufficient to induce severing, and NFL appears to be the principal target of this kinase.

The axonal transport of neurofilaments is known to slow both spatially along axons and temporally during post-natal development of myelinated axons (Hoffman et al., 1985; Hoffman et al., 1983; Jung and Brown, 2009; Xu and Tung, 2001). This contributes to the accumulation of neurofilaments that drives the expansion of myelinated axon caliber (Cleveland et al., 1991; Hoffman, 1995). The mechanism of this slowing has been attributed to an increase in phosphorylation of the carboxy-terminal tail domains of neurofilament proteins M and H (Ackerley

et al., 2003; Garcia et al., 2003; Rao et al., 2003; Sanchez et al., 2000). However, deleting these domains or mutating them to block phosphorylation did not impair neurofilament transport or accumulation *in vivo* (Garcia et al., 2009; Rao et al., 2002; Yuan et al., 2006). Thus, the role of neurofilament tail domain phosphorylation in the regulation of neurofilament transport is presently unclear. Based on the data presented above, we speculate that an alternative mechanism may be the regulation of neurofilament length. Specifically, we propose that spatial and temporal regulation of the cycle of neurofilament severing and annealing (e.g. by modulation of the activities of PKA and PP2A) could regulate neurofilament length and transport. For example, a shift in the balance of severing and annealing to favor annealing over severing during axonal maturation would result in an increase in average neurofilament length and a decrease in net transport velocity. In fact, we observed an increase in neurofilament length and a corresponding decrease in transport frequency in our cultures. However, to test this hypothesis, it will be necessary to measure neurofilament length, severing, and annealing in mature myelinated axons, which is challenge because of their high neurofilament content.

ACKNOWLEDGMENTS

We thank Chris Miller (King's College, University of London) for sharing the rat phospho- and dephospho-mimic NFL constructs, Robert Evans (University of Colorado Denver) for providing the SW13vim- cell line, Don Cleveland (University of California San Diego) for providing the NFL knockout mice originally generated by Jean-Pierre Julien (Université Laval), and Sontoria King for comments on the manuscript. This work was supported by National Institutes of Health Grants R01 NS038526, P30 NS104177, P30 NS104177, and S10 OD010383 to A.B., and by a grant from the Takeda Science Foundation to A.U.. The authors declare that they have no competing financial interests.

REFERENCES

Ackerley, S., P. Thornhill, A.J. Grierson, J. Brownlees, B.H. Anderton, P.N. Leigh, C.E. Shaw, and C.C. Miller. 2003. Neurofilament heavy chain side arm phosphorylation regulates axonal transport of neurofilaments. *J. Cell Biol.* 161:489-495.

Ando, S., K. Tanabe, Y. Gonda, C. Sato, and M. Inagaki. 1989. Domain- and sequence-specific phosphorylation of vimentin induces disassembly of the filament structure. *Biochemistry*. 28:2974-2979.

Ando, S., T. Tokui, T. Yano, and M. Inagaki. 1996. Keratin 8 phosphorylation in vitro by cAMP-dependent protein kinase occurs within the amino- and carboxyl-terminal end domains. *Biochem. Biophys. Res. Commun.* 221:67-71.

Betts, J.C., W.P. Blackstock, M.A. Ward, and B.H. Anderton. 1997. Identification of phosphorylation sites on neurofilament proteins by nanoelectrospray mass spectrometry. *J. Biol. Chem.* 272:12922-12927.

Black, M.M., P. Keyser, and E. Sobel. 1986. Interval between the synthesis and assembly of cytoskeletal proteins in cultured neurons. *J. Neurosci.* 6:1004-1012.

Brewer, G.J., M.D. Boehler, T.T. Jones, and B.C. Wheeler. 2008. NbActiv4 medium improvement to Neurobasal/B27 increases neuron synapse densities and network spike rates on multielectrode arrays. *J. Neurosci. Methods*. 170:181-187.

Brown, A. 1997. Visualization of single neurofilaments by immunofluorescence microscopy of splayed axonal cytoskeletons. *Cell Motil. Cytoskel.* 38:133-145.

Brown, A. 2000. Slow axonal transport: stop and go traffic in the axon. *Nat. Rev. Mol. Cell Biol.* 1:153-156.

Chou, Y.H., P. Opal, R.A. Quinlan, and R.D. Goldman. 1996. The relative roles of specific N- and C-terminal phosphorylation sites in the disassembly of intermediate filament in mitotic BHK-21 cells. *J. Cell Sci.* 109 (Pt 4):817-826.

Cleveland, D.W., M.J. Monteiro, P.C. Wong, S.R. Gill, J.D. Gearhart, and P.N. Hoffman. 1991. Involvement of neurofilaments in the radial growth of axons. *J. Cell Sci.* Suppl. 15:85-95.

Cleverley, K.E., J.C. Betts, W.P. Blackstock, J.M. Gallo, and B.H. Anderton. 1998. Identification of novel in vitro PKA phosphorylation sites on the low and middle molecular mass neurofilament subunits by mass spectrometry. *Biochemistry*. 37:3917-3930.

Colakoglu, G., and A. Brown. 2009. Intermediate filaments exchange subunits along their length and elongate by end-to-end annealing. *J. Cell Biol.* 185:769-777.

Eriksson, J.E., T. He, A.V. Trejo-Skalli, A.S. Harmala-Brasken, J. Hellman, Y.H. Chou, and R.D. Goldman. 2004. Specific in vivo phosphorylation sites determine the assembly dynamics of vimentin intermediate filaments. *J. Cell Sci.* 117:919-932.

Evans, R.M. 1988. Cyclic AMP-dependent protein kinase-induced vimentin filament disassembly involves modification of the N-terminal domain of intermediate filament subunits. *FEBS Lett.* 234:73-78.

Fenn, J.D., C.M. Johnson, J. Peng, P. Jung, and A. Brown. 2018a. Kymograph analysis with high temporal resolution reveals new features of neurofilament transport kinetics. *Cytoskeleton (Hoboken)*. 75:22-41.

Fenn, J.D., P.C. Monsma, and A. Brown. 2018b. Axonal neurofilaments exhibit frequent and complex folding behaviors. *Cytoskeleton (Hoboken)*. 75:258-280.

Francis, F., S. Roy, S.T. Brady, and M.M. Black. 2005. Transport of neurofilaments in growing axons requires microtubules but not actin filaments. *J. Neurosci. Res.* 79:442-450.

Garcia, M.L., C.S. Lobsiger, S.B. Shah, T.J. Deerinck, J. Crum, D. Young, C.M. Ward, T.O. Crawford, T. Gotow, Y. Uchiyama, M.H. Ellisman, N.A. Calcutt, and D.W. Cleveland. 2003. NF-M is an essential target for the myelin-directed "outside-in" signaling cascade that mediates radial axonal growth. *J. Cell Biol.* 163:1011-1020.

Garcia, M.L., M.V. Rao, J. Fujimoto, V.B. Garcia, S.B. Shah, J. Crum, T. Gotow, Y. Uchiyama, M. Ellisman, N.A. Calcutt, and D.W. Cleveland. 2009. Phosphorylation of highly conserved neurofilament medium KSP repeats is not required for myelin-dependent radial axonal growth. *J. Neurosci.* 29:1277-1284.

Geisler, N., U. Plessmann, and K. Weber. 1985. The complete amino acid sequence of the major mammalian neurofilament protein (NF-L). *FEBS Lett.* 182:475-478.

Giasson, B.I., J.A. Cromlish, E.S. Athlan, and W.E. Mushynski. 1996. Activation of cyclic AMP-dependent protein kinase in okadaic acid-treated neurons potentiates neurofilament fragmentation and stimulates phosphorylation of Ser^2 in the low-molecular-mass neurofilament subunit. *J. Neurochem.* 66:1207-1213.

Giasson, B.I., and W.E. Mushynski. 1998. Intermediate filament disassembly in cultured dorsal root ganglion neurons is associated with amino-terminal head domain phosphorylation of specific subunits. *J. Neurochem.* 70:1869-1875.

Gill, S.R., P.C. Wong, M.J. Monteiro, and D.W. Cleveland. 1990. Assembly properties of dominant and recessive mutations in the small mouse neurofilament (NF-L) subunit. *J. Cell Biol.* 111:2005-2019.

Gonda, Y., K. Nishizawa, S. Ando, S. Kitamura, Y. Minoura, Y. Nishi, and M. Inagaki. 1990. Involvement of protein kinase C in the regulation of assembly-disassembly of neurofilaments in vitro. *Biochem. Biophys. Res. Commun.* 167:1316-1325.

Hashimoto, R., Y. Nakamura, H. Goto, Y. Wada, S. Sakoda, K. Kaibuchi, M. Inagaki, and M. Takeda. 1998. Domain- and site-specific phosphorylation of bovine NF-L by Rho-associated kinase. *Biochem. Biophys. Res. Commun.* 245:407-411.

Hashimoto, R., Y. Nakamura, S. Komai, Y. Kashiwagi, K. Tamura, T. Goto, S. Aimoto, K. Kaibuchi, S. Shiosaka, and M. Takeda. 2000. Site-specific phosphorylation of neurofilament-L is mediated by calcium/calmodulin-dependent protein kinase II in the apical dendrites during long-term potentiation. *J. Neurochem.* 75:373-382.

He, Y., F. Francis, K.A. Myers, W. Yu, M.M. Black, and P.W. Baas. 2005. Role of cytoplasmic dynein in the axonal transport of microtubules and neurofilaments. *J. Cell Biol.* 168:697-703.

Heins, S., P.C. Wong, S. Muller, K. Goldie, D.W. Cleveland, and U. Aebi. 1993. The rod domain of NF-L determines neurofilament architecture, whereas the end domains specify filament assembly and network formation. *J. Cell Biol.* 123:1517-1533.

Herrmann, H., M. Haner, M. Brettel, N.O. Ku, and U. Aebi. 1999. Characterization of distinct early assembly units of different intermediate filament proteins. *J. Mol. Biol.* 286:1403-1420.

Hisanaga, S., Y. Gonda, M. Inagaki, A. Ikai, and N. Hirokawa. 1990. Effects of phosphorylation of the neurofilament L protein on filamentous structures. *Cell Regul.* 1:237-248.

Hisanaga, S., Y. Matsuoka, K. Nishizawa, T. Saito, M. Inagaki, and N. Hirokawa. 1994. Phosphorylation of native and reassembled neurofilaments composed of NF-L, NF-M, and NF-H by the catalytic subunit of cAMP-dependent protein kinase. *Mol. Biol. Cell*. 5:161-172.

Hoffman, P.N. 1995. The synthesis, axonal transport, and phosphorylation of neurofilaments determine axonal caliber in myelinated nerve fibers. *The Neuroscientist*. 1:76-83.

Hoffman, P.N., J.W. Griffin, B.G. Gold, and D.L. Price. 1985. Slowing of neurofilament transport and the radial growth of developing nerve fibers. *J. Neurosci.* 5:2920-2929.

Hoffman, P.N., R.J. Lasek, J.W. Griffin, and D.L. Price. 1983. Slowing of the axonal transport of neurofilament proteins during development. *J. Neurosci.* 3:1694-1700.

Hookway, C., L. Ding, M.W. Davidson, J.Z. Rappoport, G. Danuser, and V.I. Gelfand. 2015. Microtubule-dependent transport and dynamics of vimentin intermediate filaments. *Mol. Biol. Cell*. 26:1675-1686.

Huc, C., M. Escurat, K. Djabali, M. Derer, F. Landon, F. Gros, and M.M. Portier. 1989. Phosphorylation of peripherin, an intermediate filament protein, in mouse neuroblastoma

NIE 115 cell line and in sympathetic neurons. *Biochem. Biophys. Res. Commun.* 160:772-779.
Inagaki, M., Y. Nishi, K. Nishizawa, M. Matsuyama, and C. Sato. 1987. Site-specific phosphorylation induces disassembly of vimentin filaments in vitro. *Nature*. 328:649-652.
Izawa, I., and M. Inagaki. 2006. Regulatory mechanisms and functions of intermediate filaments: a study using site- and phosphorylation state-specific antibodies. *Cancer Sci.* 97:167-174.
Jung, P., and A. Brown. 2009. Modeling the slowing of neurofilament transport along the mouse sciatic nerve. *Phys. Biol.* 6:046002.
Kaech, S., and G. Banker. 2006. Culturing hippocampal neurons. *Nat. Protoc.* 1:2406-2415.
Klymkowsky, M.W., L.A. Maynell, and C. Nislow. 1991. Cytokeratin phosphorylation, cytokeratin filament severing and the solubilization of the maternal mRNA Vg1. *J. Cell Biol.* 114:787-797.
Lariviere, R.C., and J.P. Julien. 2004. Functions of intermediate filaments in neuronal development and disease. *J. Neurobiol.* 58:131-148.
Leduc, C., and S. Etienne-Manneville. 2017. Regulation of microtubule-associated motors drives intermediate filament network polarization. *J. Cell Biol.* 216:1689-1703.
Lopez, C.G., O. Saldanha, K. Huber, and S. Koster. 2016. Lateral association and elongation of vimentin intermediate filament proteins: A time-resolved light-scattering study. *Proc. Natl. Acad. Sci. U. S. A.* 113:11152-11157.
Mucke, N., S. Winheim, H. Merlitz, J. Buchholz, J. Langowski, and H. Herrmann. 2016. In Vitro Assembly Kinetics of Cytoplasmic Intermediate Filaments: A Correlative Monte Carlo Simulation Study. *PloS one*. 11:e0157451.
Mukai, H., M. Toshimori, H. Shibata, M. Kitagawa, M. Shimakawa, M. Miyahara, H. Sunakawa, and Y. Ono. 1996. PKN associates and phosphorylates the head-rod domain of neurofilament protein. *J. Biol. Chem.* 271:9816-9822.
Nakamura, Y., R. Hashimoto, Y. Kashiwagi, S. Aimoto, E. Fukusho, N. Matsumoto, T. Kudo, and M. Takeda. 2000. Major phosphorylation site (Ser^{55}) of neurofilament L by cyclic AMP-dependent protein kinase in rat primary neuronal culture. *Journal of Neurochemistry* 74:949-959.
Preibisch, S., S. Saalfeld, and P. Tomancak. 2009. Globally optimal stitching of tiled 3D microscopic image acquisitions. *Bioinformatics*. 25:1463-1465.
Rao, M.V., J. Campbell, A. Yuan, A. Kumar, T. Gotow, Y. Uchiyama, and R.A. Nixon. 2003. The neurofilament middle molecular mass subunit carboxyl-terminal tail domains is essential for the radial growth and cytoskeletal architecture of axons but not for regulating neurofilament transport rate. *J. Cell Biol.* 163:1021-1031.
Rao, M.V., M.L. Garcia, Y. Miyazaki, T. Gotow, A. Yuan, S. Mattina, C.M. Ward, N.A. Calcutt, Y. Uchiyama, R.A. Nixon, and D.W. Cleveland. 2002. Gene replacement in mice reveals that the heavily phosphorylated tail of neurofilament heavy subunit does not affect axonal caliber or the transit of cargoes in slow axonal transport. *J. Cell Biol.* 158:681-693.
Robert, A., P. Tian, S.A. Adam, M. Kittisopikul, K. Jaqaman, R.D. Goldman, and V.I. Gelfand. 2019. Kinesin-dependent transport of keratin filaments: a unified mechanism for intermediate filament transport. *FASEB J.* 33:388-399.
Roy, S., P. Coffee, G. Smith, R.K.H. Liem, S.T. Brady, and M.M. Black. 2000. Neurofilaments are transported rapidly but intermittently in axons: implications for slow axonal transport. *J. Neurosci.* 20:6849-6861.
Sacher, M.G., E.S. Athlan, and W.E. Mushynski. 1992. Okadaic acid induces the rapid and reversible disruption of the neurofilament network in rat dorsal root ganglion neurons. *Biochem. Biophys. Res. Commun.* 186:524-530.
Sacher, M.G., E.S. Athlan, and W.E. Mushynski. 1994. Increased phosphorylation of the amino-terminal domain of the low molecular weight neurofilament subunit in okadaic acid-treated neurons. *J. Biol. Chem.* 269:18480-18484.

Saito, T., H. Shima, Y. Osawa, M. Nagao, B.A. Hemmings, T. Kishimoto, and S. Hisanaga. 1995. Neurofilament-associated protein phosphatase 2A: its possible role in preserving neurofilaments in filamentous states. *Biochemistry*. 34:7376-7384.

Sanchez, I., L. Hassinger, R.K. Sihag, D.W. Cleveland, P. Mohan, and R.A. Nixon. 2000. Local control of neurofilament accumulation during radial growth of myelinating axons in vivo: Selective role of site-specific phosphorylation. *J. Cell Biol.* 151:1013-1024.

Sarria, A.J., S.K. Nordeen, and R.M. Evans. 1990. Regulated expression of vimentin cDNA in cells in the presence and absence of a preexisting vimentin filament network. *J. Cell Biol.* 111:553-565.

Schindelin, J., I. Arganda-Carreras, E. Frise, V. Kaynig, M. Longair, T. Pietzsch, S. Preibisch, C. Rueden, S. Saalfeld, B. Schmid, J.Y. Tinevez, D.J. White, V. Hartenstein, K. Eliceiri, P. Tomancak, and A. Cardona. 2012. Fiji: an open-source platform for biological-image analysis. *Nat. Methods*. 9:676-682.

Sihag, R.K., M. Inagaki, T. Yamaguchi, T.B. Shea, and H.C. Pant. 2007. Role of phosphorylation on the structural dynamics and function of types III and IV intermediate filaments. *Exp. Cell Res.* 313:2098-2109.

Sihag, R.K., H. Jaffe, R.A. Nixon, and X. Rong. 1999. Serine-23 is a major protein kinase A phosphorylation site on the amino-terminal head domain of the middle molecular mass subunit of neurofilament proteins. *J. Neurochem.* 72:491-499.

Sihag, R.K., A.Y. Jeng, and R.A. Nixon. 1988. Phosphorylation of neurofilament proteins by protein kinase C. *FEBS Lett.* 233:181-185.

Sihag, R.K., and R.A. Nixon. 1990. Phosphorylation of the amino-terminal head domain of the middle molecular mass 145-kDa subunit of neurofilaments. Evidence for regulation by second messenger-dependent protein kinases. *J. Biol. Chem.* 265:4166-4171.

Sihag, R.K., and R.A. Nixon. 1991. Identification of Ser-55 as a major protein kinase A phosphorylation site on the 70-kDa subunit of Neurofilaments: early turnover during axonal transport. *J. Biol. Chem.* 266:18861-18867.

Stone, E.J., A. Uchida, and A. Brown. 2019. Charcot-Marie-Tooth disease Type 2E/1F mutant neurofilament proteins assemble into neurofilaments. *Cytoskeleton (Hoboken)*. 76:423-439.

Strack, S., R.S. Westphal, R.J. Colbran, F.F. Ebner, and B.E. Wadzinski. 1997. Protein serine/threonine phosphatase 1 and 2A associate with and dephosphorylate neurofilaments. *Molecular Brain Research*. 49:15-28.

Trimpin, S., A.E. Mixon, M.D. Stapels, M.Y. Kim, P.S. Spencer, and M.L. Deinzer. 2004. Identification of endogenous phosphorylation sites of bovine medium and low molecular weight neurofilament proteins by tandem mass spectrometry. *Biochemistry*. 43:2091-2105.

Uchida, A., N.H. Alami, and A. Brown. 2009. Tight functional coupling of kinesin-1A and dynein motors in the bidirectional transport of neurofilaments. *Mol. Biol. Cell*. 20:4997-5006.

Uchida, A., G. Colakoglu, L. Wang, P.C. Monsma, and A. Brown. 2013. Severing and end-to-end annealing of neurofilaments in neurons. *Proc. Natl. Acad. Sci. U. S. A.* 110:E2696–E2705

Uchida, A., P.C. Monsma, J.D. Fenn, and A. Brown. 2016. Live-cell imaging of neurofilament transport in cultured neurons. *Methods Cell Biol.* 131:21-90.

Wang, L., and A. Brown. 2001. Rapid intermittent movement of axonal neurofilaments observed by fluorescence photobleaching. *Mol. Biol. Cell*. 12:3257-3267.

Wang, L., C.-L. Ho, D. Sun, R.K.H. Liem, and A. Brown. 2000. Rapid movement of axonal neurofilaments interrupted by prolonged pauses. *Nat. Cell Biol.* 2:137-141.

Wickert, U., N. Mucke, T. Wedig, S.A. Muller, U. Aebi, and H. Herrmann. 2005. Characterization of the in vitro co-assembly process of the intermediate filament proteins vimentin and desmin: mixed polymers at all stages of assembly. *Eur. J. Cell Biol.* 84:379-391.

Winheim, S., A.R. Hieb, M. Silbermann, E.M. Surmann, T. Wedig, H. Herrmann, J. Langowski, and N. Mucke. 2011. Deconstructing the late phase of vimentin assembly by total internal reflection fluorescence microscopy (TIRFM). *PloS one*. 6:e19202.

Xu, Z., and V.W. Tung. 2001. Temporal and spatial variations in slow axonal transport velocity along peripheral motoneuron axons. *Neuroscience*. 102:193-200.

Yan, Y., and A. Brown. 2005. Neurofilament polymer transport in axons. *J. Neurosci.* 25:7014-7021.

Yates, D.M., C. Manser, K.J. De Vos, C.E. Shaw, D.M. McLoughlin, and C.C. Miller. 2009. Neurofilament subunit (NFL) head domain phosphorylation regulates axonal transport of neurofilaments. *Eur. J. Cell Biol.* 88:193-202.

Yuan, A., R.A. Nixon, and M.V. Rao. 2006. Deleting the phosphorylated tail domain of the neurofilament heavy subunit does not alter neurofilament transport rate in vivo. *Neurosci. Lett.* 393:264-268.

Zhu, Q., S. Couillard-Despres, and J.-P. Julien. 1997. Delayed maturation of regenerating myelinated axons in mice lacking neurofilaments. *Exp. Neurol.* 148:299-316.

FIGURE LEGENDS

Fig. 1. Long-range multi-field tracking of neurofilament transport

Maximum intensity projection of a montage of images from a time-lapse movie of a neonatal rat cortical neuron after 8 days in culture, showing the trajectory of a neurofilament along an axon. The microscope stage was moved 10 times during the course of the movie, allowing the moving filament to be tracked for a distance of approximately 420 μm over a period of 12.4 min (248 images acquired at 3 s time intervals). The images were aligned using the encoded microscope stage coordinates to create a movie montage comprised of 11 distinct overlapping fields (yellow boxes). Each field measures approximately 82 x 82 μm, corresponding to the field of view of the camera (512 x 512 pixels). The inset is a region of one image plane at higher magnification, showing the tracked filament. Scale bar=20 μm in main figure and 5 μm in inset.

Fig. 2. Example trajectories of long and short neurofilaments

A-D. Representative trajectories of four short filaments ranging from 2.5 to 6.9 μm in length. **E-H.** Representative trajectories of four long filaments ranging from 18.9 to 31.3 μm in length. Data from time-lapse movies of neonatal rat cortical neurons after 8-10 days in culture. Distance along the axon is plotted versus time, with anterograde movements considered positive and retrograde movements negative. The lengths of the filaments are marked on the plots. Each filament was tracked for up to 30 min (1800 s). In five cases, the tracking was terminated early for one of three reasons: the filament reached one end of the axon or the other (A,D), annealed with another filament (C), or severed (E,F), as indicated by the arrows on the plots. Note that the short filaments moved rapidly and persistently in the anterograde or retrograde direction, whereas the long filaments also moved rapidly, but paused and reversed direction more frequently.

Fig. 3. Length-dependence of net neurofilament transport velocity

A-F. Scatter plots of net velocity, net distance moved, and tracking duration plotted against filament length for filaments that were tracked for up to 30 min each (A,C,E; n=93 neurofilaments) and for the subset of those filaments that were tracked for at least 8 min each (B,D,F; n=65 neurofilaments). Data from time-lapse movies of neonatal rat cortical neurons after 8-10 days in culture. The net velocity was calculated as the net distance moved (distance along the axon from the start of the trajectory until the end) divided by tracking duration (duration that the filament was tracked). The red curves represent logarithmic curve fits. **G,H.** Corresponding bar graphs of the average net velocity binned into short (0-10 μm), medium (10-20 μm), and long (20-50 μm)

categories based on the filament length. The number of filaments in each category is written on the plot. Note that the average net velocity declined with increasing neurofilament length for filaments that moved in both net anterograde and net retrograde directions.

Fig. 4. Long neurofilaments pause and reverse more often

A-C. Box-and-whisker plots of percent time pausing, persistence, and peak velocity for the subset of filaments that were tracked for at least 8 min in Fig. 3 (n=65 neurofilaments). The data were binned into short (0-10 μm), medium (10-20 μm), and long (20-50 μm) categories based on the filament length. The number of filaments in each length category is indicated on the plots. Each box represents the range for the middle 50% of the data, with the median displayed as a horizontal line. The whiskers represent the minimum and maximum values within the data set that are greater than or less than 1.5 times the interquartile distance. Points outside of this range (outliers) are displayed as open circles. Percent time pausing was calculated as the proportion of the time that each filament spent pausing, calculated using a pause threshold of 0.15 μm/s. Persistence was calculated as the net distance moved (distance along the axon from the start of the trajectory until the end) divided by the total distance moved (irrespective of direction). Peak velocity was calculated as the maximum interval velocity for each filament. Note that long filaments spent more time pausing and moved less persistently than short filaments, but with similar peak velocities. The p-values were obtained using the Mann-Whitney-Wilcoxon test.

Fig. 5. Length-dependence of neurofilament severing and annealing

A,B. Excerpts from two time-lapse movies documenting examples of annealing (A) and severing (B) events (see also Movies S2 and S3, respectively). Time is shown in seconds relative to the first frame in the figure. Proximal is left and distal is right. In A, filament “a” moved anterogradely initially (t=0-21s) and then paused and folded along part of its length resulting in an increase in brightness at its proximal end. Note that a portion of this filament was out of focus because the axon passed slightly outside the plane of focus at that point. Filament “b” then moved retrogradely into the field of view from the right and overlapped filament “a” (t=33s). The two filaments then annealed and the resulting daughter filament moved retrogradely, stretching out as it did so (t=63-129s). Filament lengths: 20.8 μm (a), 6.3 μm (b), 27.5 μm (a+b). In B, filament “c” was initially paused and partially folded (t=0s) and then stretched out as it moved retrogradely (t=9-99s). The filament then paused (t=99-186s) before severing (t=195s). The leading filament fragment (“c1”) continued to move retrogradely and the trailing fragment (“c2”) folded back on itself (note the increase in brightness in the folded region) and remained paused. Filament lengths: 29 μm (c),

7.1 μm (c1), 21.6 μm (c2). Scale bar=10μm. **C,D.** Histograms of the annealing and severing frequency for short (0-10 μm), medium (10-20 μm), and long (20-50 μm) filaments. Data from 97 movies (total=141 neurofilaments observed for 32 hr; average time-lapse movie duration=13.6 min) including the 76 movies (93 neurofilaments) analyzed in Fig. 3 plus an additional 21 movies (48 neurofilaments) that were excluded from that dataset due to ambiguity in the axon orientation or that were analyzed with time-lapse intervals of 2 s. The number of filaments tracked and the total observation time for those filaments is marked on the plots for each length category. The filament length corresponding to each severing or annealing event was taken to be the length of the tracked filament before the event. The annealing and severing frequencies were calculated as the number of end-to-end annealing or severing events observed per neurofilament per hr of observation. Note that short filaments annealed more frequently than long filaments and that long filaments severed more frequently than short filaments.

Fig. 6. Phospho- and dephospho-mimics of NFL assemble into neurofilaments

A-H. Spinning disk confocal microscopy of neurofilaments in cell bodies (A-D) and axons (E-H) of neonatal rat cortical neurons expressing $NFL^{S2,55,57,66A}$-myc (dephospho-mimic) or $NFL^{S2,55,57,66D}$-myc (phospho-mimic), immunostained for myc and NFM 10-11 days after plating. The colocalization of myc and NFM confirms that the mutant NFL co-assembled into neurofilaments with NFM. **I,J.** Live wide-field imaging of axonal neurofilaments in axons of neurons expressing $NFL^{S2,55,57,66A}$-GFP or $NFL^{S2,55,57,66D}$-GFP 10 days after plating. Note the uniform incorporation of the mutant proteins along the neurofilaments and the absence of aggregates or diffuse fluorescence, which confirms that the mutant proteins assemble fully into neurofilaments. On average, the neurofilaments containing the phospho-mimic mutant were shorter, which is confirmed by the quantitative analysis in Fig. 7. Scale bars= 5 μm. **K.** Schematic showing the location of the mutated serine residues in the N-terminal head domain of the NFL protein. Note that the numbering of the residues ignores the N-terminal methionine (see explanation in Methods).

Fig. 7. Phospho- and dephospho-mimics of NFL alter neurofilament length and transport

A-C. Histograms of the neurofilament length in neonatal rat cortical neurons expressing either wild type NFL-GFP (A), $NFL^{S2,55,57,66A}$-GFP (dephospho-mimic) (B), or $NFL^{S2,55,57,66D}$-GFP (phospho-mimic) (C). The lengths were measured for moving filaments in time-lapse movies acquired after 8 days in culture (15 movies, average duration=15 min, total neurofilaments measured=376). The filaments exhibited an approximately exponential distribution as we have

described previously (Fenn et al., 2018a), but the average length was longer in neurons expressing the dephospho-mimic and shorter in neurons expressing the phospho-mimic. **D-F.** Histograms of the frequency of neurofilament movement in neonatal rat cortical neurons expressing either $NFL^{S2,55,57,66A}$-GFP (dephospho-mimic; D), wild type NFL-GFP (E), or $NFL^{S2,55,57,66D}$-GFP (phospho-mimic; F) and observed by time-lapse imaging after 8 days in culture. Data from time-lapse movies of neonatal rat cortical neurons after 8 days in culture (21 movies, average duration=30 min, 174 axons, total neurofilaments tracked=491). The frequency was calculated by counting the number of filaments that crossed the midpoint of the longest gap in the neurofilament array of each axon in each movie and then dividing the number by the duration of the movie (see Methods). Note that the average frequency of neurofilament movement was higher in neurons expressing the phospho-mimic compared to neurons expressing the dephospho-mimic.

Fig. 8. Phospho- and dephospho-mimics of NFL alter neurofilament annealing and severing frequency

A-D. Histograms of the frequency of annealing events (A,B) and severing events (C,D) in axons neonatal rat cortical neurons expressing either $NFL^{S2,55,57,66A}$-GFP (dephospho-mimic) (A,C) or $NFL^{S2,55,57,66D}$-GFP (phospho-mimic) (B,D) and observed by time-lapse imaging after 8-10 days in culture (141 movies, average duration=24 min, total neurofilaments tracked=244). The filament length corresponding to each severing or annealing event was taken to be the length of the tracked filament before the event. The data were binned into short (0-10 μm), medium (10-20 μm), and long filaments. Note that the long filament category was 20-50 μm for the phospho-mimic and 20-120 μm for the dephospho-mimic. This is because we encountered four filaments in the latter condition that were longer than 50 μm (specifically 57, 61, 100, and 112 μm). The number of filaments tracked and the total observation time for those filaments is marked on the plots for each length category (total=122 filaments tracked for a total of 31.2 hr for the dephospho-mimic; total=122 filaments tracked for a total of 25.1 hr for the phospho-mimic). Note that the phospho-mimic impairs the annealing frequency of short filaments and enhances the severing frequency at all filament lengths (compare to Fig. 5C). In contrast, the dephospho-mimic enhances the annealing frequency for short and medium length filaments and suppresses the severing frequency of long filaments (compare to Fig. 5D). **E,F.** Average net velocities for short (0-10 μm), medium (10-20 μm), and long (20-50 μm for the phospho-mimic and 20-120 μm for the dephospho-mimic) filaments in neonatal rat cortical neurons expressing either $NFL^{S2,55,57,66A}$-GFP (dephospho-mimic) (A) or $NFL^{S2,55,57,66D}$-GFP (phospho-mimic) (B). Data from the time-lapse

movies recorded for Fig. 8 but including only neurofilaments that were tracked for at least 8 min (116 movies, 154 neurofilaments) in order to focus on the long-term kinetic behavior, as described above. The number of filaments tracked in both anterograde and retrograde net directions is marked on the plots. Note that the net velocity declined with increasing filament length, and this was similar for the two mutants and for filaments moving in both net directions. Thus, the effects of the NFL phospho- and dephospho-mimics on neurofilament transport are due to their effects on neurofilament length.

Fig. 9. Dephospho-mimic NFL protects neurofilaments against the effect of protein kinase A activators

A-D. Histograms of neurofilament length in neonatal mouse cortical neurons from NFL knockout mice after 8-10 days in culture (77 movies, average duration=15 min, total of 1768 neurofilaments tracked). The neurons were transfected with wild type NFL-GFP (A,C) or the dephospho-mimic $NFL^{S2,55,57,66A}$-GFP (B,D) and then treated with vehicle (A,B) or 8-bromo-cAMP and okadaic acid, which are activators of protein kinase A (C,D). The schematic above the plots shows the experimental timeline, which involved pre-treatment for 3 hr with 8-bromo-cAMP, treatment for 2 hr in the presence of 8-bromo-cAMP plus okadaic acid, and imaging for up to 3 hr in the continued presence of these reagents. Note that the treatment reduced neurofilament length in neurons expressing wild type NFL, but not in neurons expressing the dephospho-mimic.

Fig. 10. Regulation of neurofilament transport by a dynamic cycle of neurofilament severing and annealing

A. Schematic diagram of the cycle of neurofilament severing and annealing described in this study. Long neurofilaments move rapidly but often pause for prolonged periods and often reverse direction, which results in little net movement. Severing generates shorter filaments that move more persistently in either the anterograde or retrograde direction, pausing and reversing less often. Annealing generates longer filaments. Short filaments anneal more frequently than long filaments, whereas long filaments sever more frequently than short filaments. The result is a dynamic cycle of severing and annealing that influences neurofilament transport kinetics.

SUPPLEMENTAL DATA

Fig. S1. Phospho- and dephospho-mimics of NFL assemble into neurofilaments in SW13vim- cells

Spinning disk confocal microscopy of SW13vim- cells, which lack endogenous cytoplasmic intermediate filaments, co-expressing $NFL^{S2,55,57,66A}$-myc (dephospho-mimic) and NFM (A,C,E) or $NFL^{S2,55,57,66D}$-myc (phospho-mimic) and NFM (B,D,F). The cells were transfected 24 hr after plating and fixed and immunostained for NFM and myc 16 hr later. The overlay panels (E,F) show the NFM in green and the myc in magenta. Scale bar=10μm.

Fig. S2. Accumulation of neurofilaments in axons of cortical neurons expressing dephospho-mimic NFL after 2-3 weeks in culture

Cortical neurons transfected with the dephospho-mimic $NFL^{S2,55,57,66A}$-GFP or the phospho-mimic $NFL^{S2,55,57,66D}$-GFP and then imaged live 16-21 days later using the spinning disk confocal microscope in widefield bypass mode. Overlapping images were acquired along the entire length of multiple axons. Montages were created in the FIJI distribution package of ImageJ (Schindelin et al., 2012) using the Pairwise Stitching plug-in (Preibisch et al., 2009). A. Examples of montages of axons expressing the dephospho-mimic $NFL^{S2,55,57,66A}$-GFP (20 overlapping fields) or the phospho-mimic $NFL^{S2,55,57,66D}$-GFP (19 overlapping fields). Note the axon expressing the dephospho-mimic is brighter and wider and brighter, indicating a higher neurofilament content. The images were all acquired with the same exposure and subjected to the same intensity scaling. Scale bars=25 μm. B. Histograms showing the average axon width for axons expressing $NFL^{S2,55,57,66A}$-GFP dephospho-mimic (n=5) or $NFL^{S2,55,57,66D}$-GFP phospho-mimic (n=5). The axon width was taken to be the width at half-height on a linear intensity profile (line-width=11 pixels) drawn perpendicular to the long axis of the axon, measured at the mid-point of the axon within each image of the montage, i.e. at approximately 200-300 μm intervals along the axons. Shapiro-Wilk's test did not reveal a significant deviation from normality ($p=0.191$ for $NFL^{S2,55,57,66A}$-GFP; $p=0.478$ for $NFL^{S2,55,57,66D}$-GFP). Levene's test revealed no significant difference in the variance ($p=0.198$). The data were compared using an unpaired t-test for equal variances ($p<0.001$).

Fig. S3. Dephospho-mimic NFL partially protects neurofilaments against the effect of protein kinase A activators in rat cortical neurons

A-D. Histograms of neurofilament length in neonatal rat cortical neurons after 12-14 days in culture (148 movies, average duration=15 min, total of 2,212 neurofilaments tracked). The neurons were transfected with wild type rat NFL-GFP (AC,E,G) or the dephospho-mimic rat $NFL^{S2,55,57,66A}$-GFP (B,D,F,H) and treated with vehicle (A,B), 8-bromo-cAMP (C,D), okadaic acid (E,F), or 8-bromo-cAMP plus okadaic acid (G,H). The schematic above the plots shows the experimental timeline, which involved pre-treatment for 3 hr with 8-bromo-cAMP, treatment for 2 hr in the presence of okadaic acid plus 8-bromo-cAMP, and then imaging for up to 3 hr in the continued presence of these reagents. Note that the treatment with either cAMP or okadaic acid reduced neurofilament length in neurons expressing wild type NFL (C,E), and the effect was more marked for neurons treated with cAMP and okadaic acid together (G). The same treatments also reduced neurofilament length in neurons expressing the dephospho-mimic, but the extent of the reduction was less (D,F,H). Note that the number of filaments measured in C,D,E and F was much lower than in A,B,G and H.

Table S1. Neurofilament length and transport frequency versus age in culture

Average neurofilament length and transport frequency in neonatal rat cortical neurons expressing either wild type NFL-GFP (A), $NFL^{S2,55,57,66A}$-GFP (dephospho-mimic) (B), or $NFL^{S2,55,57,66D}$-GFP (phospho-mimic) (C). The lengths were measured for moving filaments in time-lapse movies acquired after 8 days in culture (15 movies, average duration=15 min, total neurofilaments measured=376). The filaments exhibited an approximately exponential distribution as we have described previously (Fenn et al., 2018a), but the average length was longer in neurons expressing the dephospho-mimic and shorter in neurons expressing the phospho-mimic. **D,E.** Histograms of the frequency of neurofilament movement in neonatal rat cortical neurons expressing either $NFL^{S2,55,57,66A}$-GFP (dephospho-mimic) (D) or $NFL^{S2,55,57,66D}$-GFP (phospho-mimic) (E) and observed by time-lapse imaging after 8 days in culture. Data from time-lapse movies of neonatal rat cortical neurons after 8 days in culture (21 movies, average duration=30 min, 174 axons, total neurofilaments tracked=491). The frequency was calculated by counting the number of filaments that crossed the midpoint of the longest gap in the neurofilament array of each axon in each movie and then dividing the number by the duration of the movie (see Methods). Note that the average frequency of neurofilament movement was higher in neurons expressing the phospho-mimic compared to neurons expressing the dephospho-mimic.

MOVIE LEGENDS

Movie S1. Long-range multi-field tracking of a neurofilament

Multi-field time-lapse movie of a cortical neuron expressing GFP-NFM, showing a short neurofilament (length=4.3 μm) that moves retrogradely along the axon, eventually entering the cell body. The filament is to the lower left of the center of the field of view at the start of the movie. Note that the filament moves persistently in one direction, pausing infrequently, and that it is not visible at 01:48 to 2:03 and 04:14 to 04:45 because the axon passes out of the plane of focus as it courses over other cells at these locations. At 02:03, the filament passes another short filament that is pausing. At 03:06, the filament passes a short filament that is moving in the opposite (anterograde) direction. At 05:09, the filament passes a pausing filament, which subsequently moves in the opposite (anterograde) direction. The movie ends at 06:09 when the filament enters the cell body. Dimensions of field: 318 x 207 μm. Proximal is right, distal is left. Time-lapse interval: 3 sec. Time stamp min:sec. Time compression 21:1.

Movie S2. An annealing event

Excerpt from a multi-field time-lapse movie of a cortical neuron expressing GFP-NFM, showing a long neurofilament (length=20.8 μm) that moves anterogradely initially. The filament is in the center of the field of view at the start of the movie. The filament pauses at 03:00 and then anneals at its proximal end with a short retrogradely moving neurofilament (length=6.3 μm). The resulting daughter filament (length=27.5 μm) then shuttles back and forth repeatedly from 03:00 to 09:00, as if engaged in a tug-of-war, before moving persistently in a retrograde direction. Dimensions of field: 171 x 170 μm. Proximal is upper left, distal is lower right. Time-lapse interval: 3 sec. Time stamp min:sec. Time compression 21:1.

Movie S3. A severing event

Excerpt from a multi-field time-lapse movie of a cortical neuron expressing GFP-NFM, showing a long neurofilament (length=29 μm). The filament is in the center of the field of view at the start of the movie. The filament moves anterogradely in a folded configuration initially, fully unfolding at 03:51. The filament then appears to sever at 04:15, though this is not clearly evident until the two daughter filaments separate at 05:21. The shorter (proximal) daughter filament (length=7.1 μm) moves away in a retrograde direction, then the longer (distal) daughter filament (length=21.6 μm) folds up on itself at 05:36 before unfolding and resuming anterograde movement at 07:12.

Dimensions of field: 118 x 133 μm. Proximal is lower left, distal is upper right. Time-lapse interval: 3 sec. Time stamp min:sec. Time compression 21:1.

Movie S4. Rapid persistent movement of a short neurofilament

Multi-field time-lapse movie of a cortical neuron expressing GFP-NFM, showing a short neurofilament (length=5.4 μm) that moves anterogradely. The filament is to the right of the center of the field of view at the start of the movie. It briefly folds and unfolds at 02:03 to 02:09, and then at 02:36 it catches up with a shorter filament (length=2.3 μm) that is also moving anterogradely and the two filaments anneal. The daughter filament (length=7.6 μm) continues to move anterogradely, passing another pausing filament at 03:18 to 03:30 and then at 04:24 it pauses. At 04:30 a long filament moving retrogradely overlaps the short filament and then pauses, at which point the short filament can no longer be resolved. Note that the movie drifts out of focus from 03:51 to 04:27. Dimensions of field: 347 x 101 μm. Proximal is left, distal is right. Time-lapse interval: 3 sec. Time stamp min:sec. Time compression 21:1.

Movie S5. Frequent pausing and reversal of a long neurofilament

Multi-field time-lapse movie of a cortical neuron expressing GFP-NFM, showing a long neurofilament (length=27.9 μm) that severs twice. The filament is in the center of the field of view at the start of the movie, partially overlapping one or more pausing neurofilaments. The filament moves past these pausing filaments in a net retrograde direction, frequently pausing and reversing direction. Note that the filament remains fully extended during these bidirectional movements, as if pulled alternately at one end and then the other (Fenn et al., 2018b), and that it passes several shorter filaments moving in the opposite (anterograde) direction around 04:42 and 08:51. The filaments occasionally pass out of the plane of focus at locations where the axon crosses another cell. At around 10:06, the filament begins to move persistently back in the anterograde direction, passing several other pausing filaments starting at 13:57 and eventually pauses at 15:30 close to where it started and partially overlapping another pausing filament. At 17:39 the latter filament appears to anneal with a very short filament moving anterogradely and then the daughter filament moves away in the anterograde direction. At 18:30, the filament of interest folds back on itself. Two shorter filaments moving in the retrograde direction then overlap the filament of interest at 20:09 and 21:03, pausing and then moving away at 21:06 and 21:33, respectively. At some point during this period of folding and overlap, the filament of interest severs twice. This becomes evident when the daughter fragments move apart in the anterograde direction at 21:42 and 22:24, giving rise first to three fragments (lengths=10.6, 6.0 and 11.0 μm)

that can be resolved from each other in the final frame. Dimensions of field: 310 x 166 μm. Proximal is right, distal is left. Time-lapse interval: 3 sec. Time stamp min:sec. Time compression 21:1.

Movie S6. Movement of neurofilaments expressing the NFL dephospho-mimic

Fixed-field time-lapse movie of cortical neurons expressing the $NFL^{S2,55,57,66A}$-GFP dephospho-mimic. Note that the fusion protein co-assembles efficiently into neurofilaments with no detectable diffuse (unassembled) protein. On average, the filaments are longer and move less frequently than in neurons expressing wild type NFL-GFP (Movie S7). See Fig. 7 for quantification. Dimensions of field: 82 x 82 μm. Time-lapse interval: 3 sec. Time stamp min:sec. Time compression 21:1.

Movie S7. Movement of neurofilaments expressing wild type NFL

Fixed-field time-lapse movie of cortical neurons expressing wild type NFL-GFP. On average, the filaments are shorter and move more frequently than in neurons expressing the $NFL^{S2,55,57,66A}$-GFP dephospho-mimic (Movie S6). On average, the filaments are longer and move less frequently than in neurons expressing the $NFL^{S2,55,57,66D}$-GFP phospho-mimic (Movie S8). See Fig. 7 for quantification. Dimensions of field: 82 x 82 μm. Time-lapse interval: 3 sec. Time stamp min:sec. Time compression 21:1.

Movie S8. Movement of neurofilaments expressing the NFL phospho-mimic

Fixed-field time-lapse movie of cortical neurons expressing the $NFL^{S2,55,57,66D}$-GFP phospho-mimic. Note that the fusion protein co-assembles efficiently into neurofilaments with no detectable diffuse (unassembled) protein and no aggregation. On average, the filaments are shorter and move more frequently than in neurons expressing wild type NFL-GFP (Movie S7). See Fig. 7 for quantification. Dimensions of field: 82 x 82 μm. Time-lapse interval: 3 sec. Time stamp min:sec. Time compression 21:1.

Movie S9. Movement of neurofilaments expressing wild type NFL treated with cAMP and okadaic acid

Fixed-field time-lapse movie of $NFL^{-/-}$ cortical neurons expressing wild type NFL-GFP and treated with 8-bromo-cAMP and okadaic acid. On average, the filaments are shorter and move more frequently than in neurons expressing the non-phosphorylatable $NFL^{S2,55,57,66A}$-GFP dephospho-mimic and subjected to the same treatment (Movie S10). See Fig. 9 for quantification.

Dimensions of field: 82 x 82 μm. Time-lapse interval: 3 sec. Time stamp min:sec. Time compression 21:1.

Movie S10. Movement of neurofilaments expressing the NFL dephospho-mimic treated with cAMP and okadaic acid

Fixed-field time-lapse movie of $NFL^{-/-}$ cortical neurons expressing the non-phosphorylatable $NFL^{S2,55,57,66A}$-GFP dephospho-mimic and treated with 8-bromo-cAMP and okadaic acid. On average, the filaments are longer and move less frequently than in neurons expressing wild type NFL-GFP and subjected to the same treatment (Movie S9). See Fig. 9 for quantification. Dimensions of field: 82 x 82 μm. Time-lapse interval: 3 sec. Time stamp min:sec. Time compression 21:1.

Fig. 1

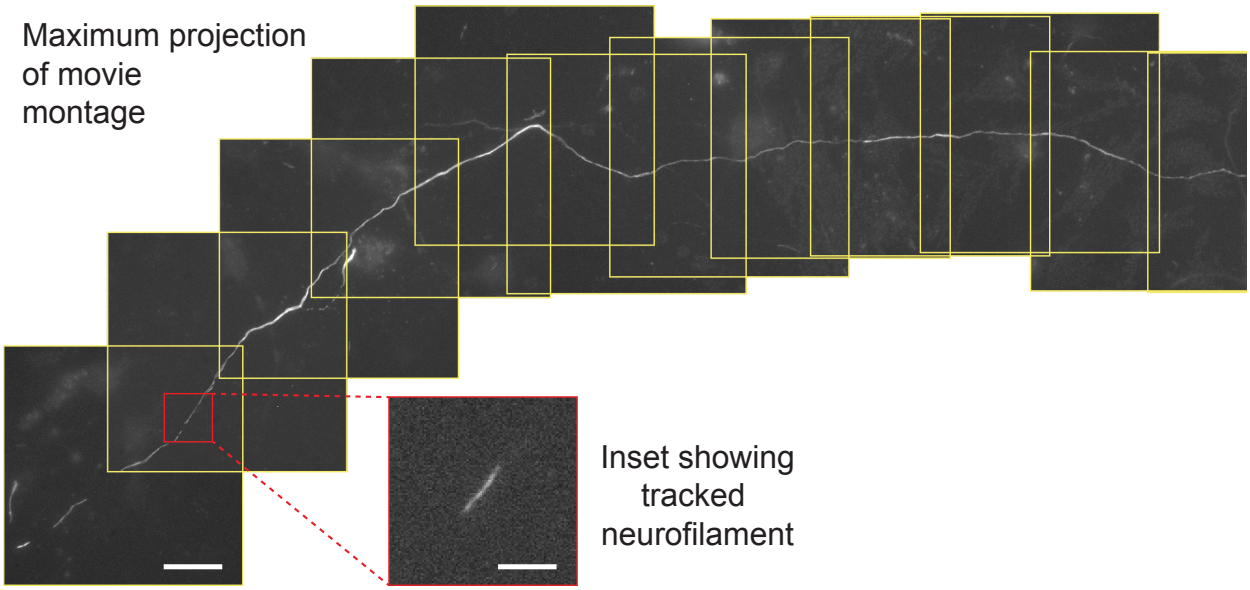
Maximum projection
of movie
montage
Inset showing
tracked
neurofilament

Fig. 2

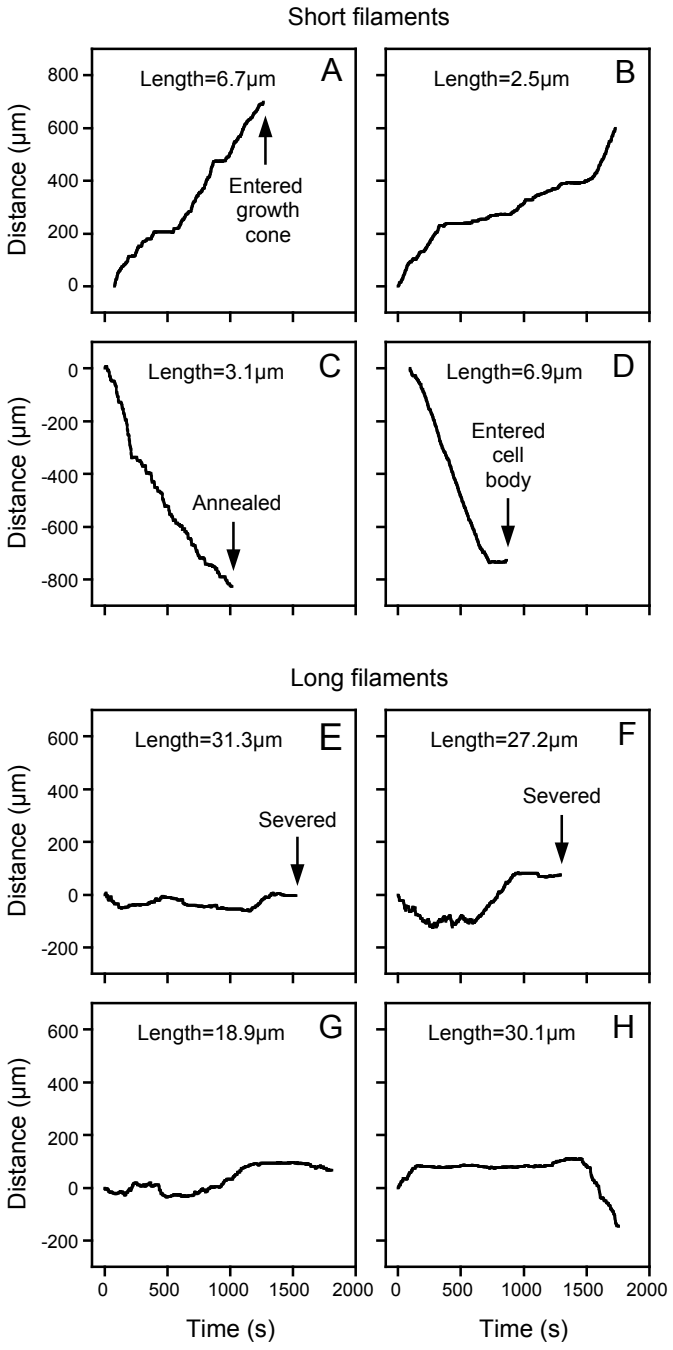
Short filaments
Length=6.7μm
A
Entered growth cone
Length=2.5μm
B
Length=3.1μm
C
Annealed
Length=6.9μm
D
Entered cell body
Distance (μm)
Long filaments
Length=31.3μm
E
Severed
Length=27.2μm
F
Severed
Length=18.9μm
G
Length=30.1μm
H
Time (s)

Fig. 3

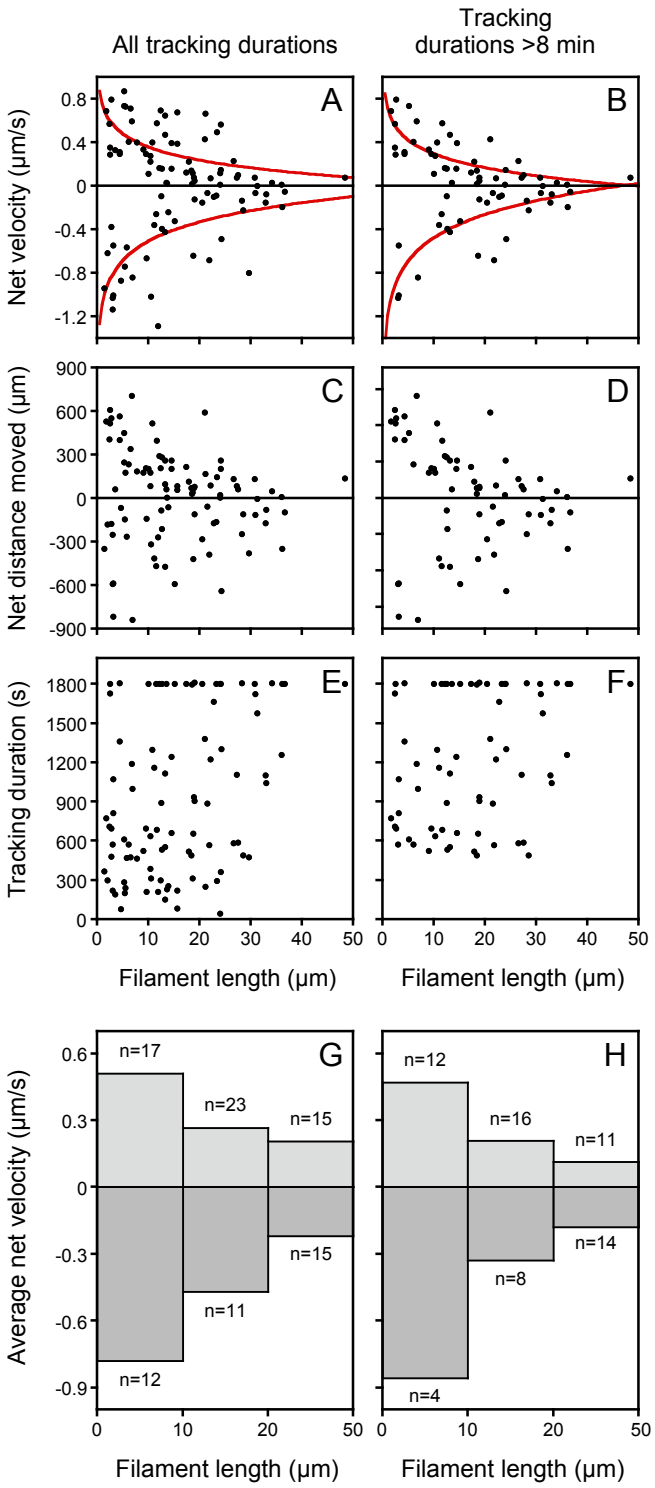
All tracking durations
Tracking durations >8 min
A
B
C
D
E
F
G
H
Net velocity (µm/s)
Net distance moved (µm)
Tracking duration (s)
Average net velocity (µm/s)
Filament length (µm)
n=17
n=23
n=15
n=15
n=11
n=12
n=12
n=16
n=11
n=14
n=8
n=4

Fig. 4

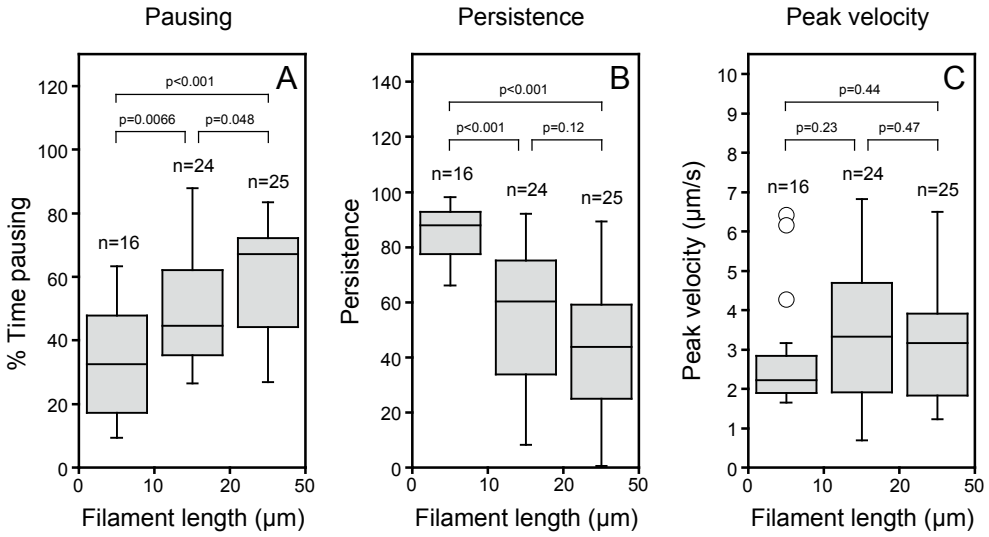
Pausing
Persistence
Peak velocity
A
B
C
p<0.001
p=0.0066
p=0.048
p<0.001
p<0.001
p=0.12
p=0.44
p=0.23
p=0.47
n=16
n=24
n=25
% Time pausing
Persistence
Peak velocity (µm/s)
Filament length (µm)

Fig. 5

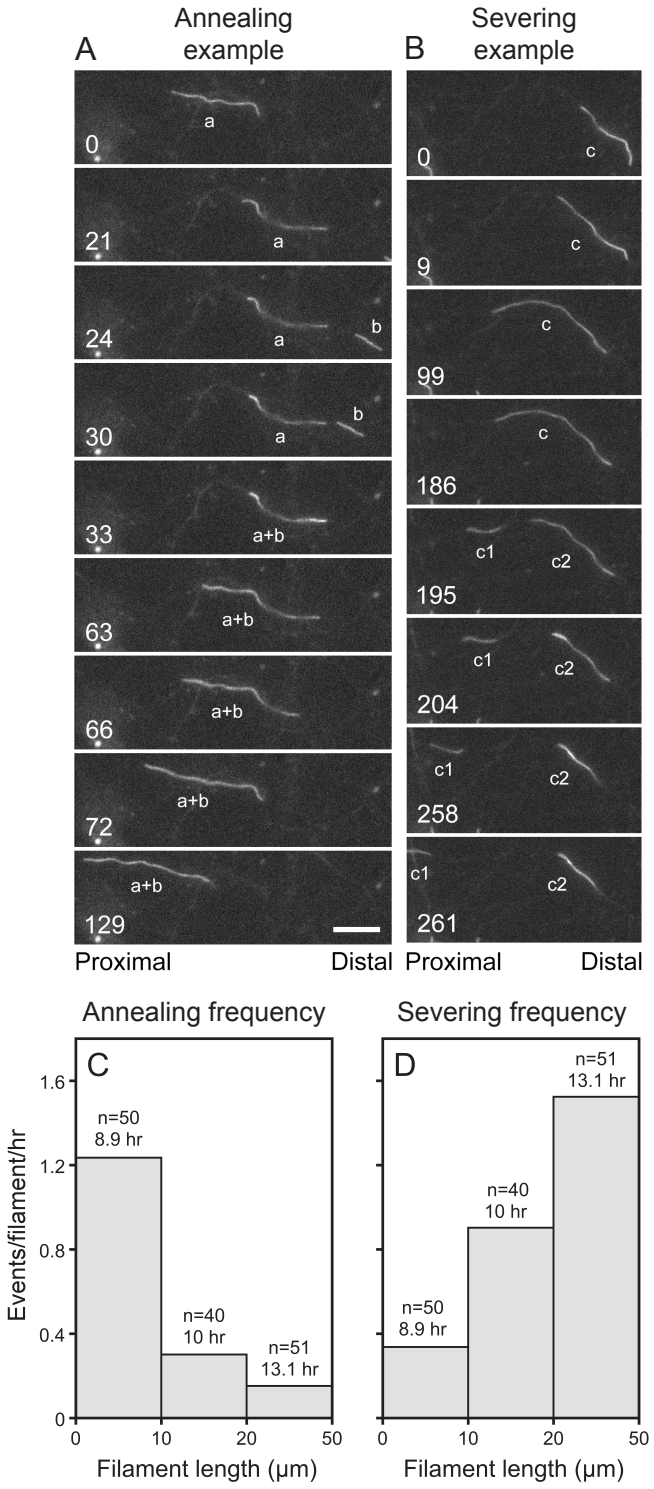
A
Annealing example
B
Severing example
0
21
24
30
33
63
66
72
129
a
b
a+b
c
9
99
186
195
204
258
261
c1
c2
Proximal
Distal
Annealing frequency
Severing frequency
C
D
Events/filament/hr
1.6
1.2
0.8
0.4
0
n=50
8.9 hr
n=40
10 hr
n=51
13.1 hr
Filament length (μm)
0
10
20
50

Fig. 6

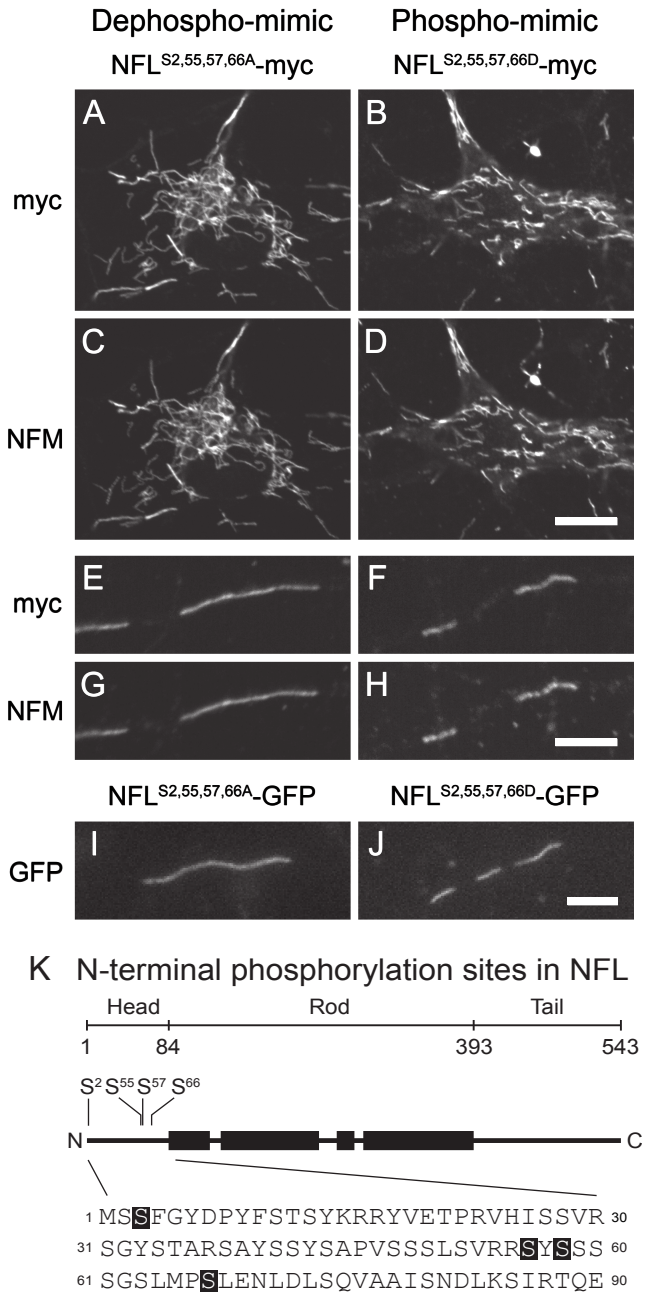
Dephospho-mimic
Phospho-mimic
NFL S2,55,57,66A-myc
NFL S2,55,57,66D-myc
A
B
myc
C
D
NFM
E
F
myc
G
H
NFM
NFL S2,55,57,66A-GFP
NFL S2,55,57,66D-GFP
I
J
GFP
K N-terminal phosphorylation sites in NFL
Head
Rod
Tail
1
84
393
543
S2 S55 S57 S66
N
C
1 MSSFGYDPYFSTSYKRRYVETPRVHISSVR 30
31 SGYSTARSAYSSYSAPVSSSLSVRRSYSSS 60
61 SGSLMPSLENLDLSQVAAISNDLKSIRTQE 90

Fig. 7

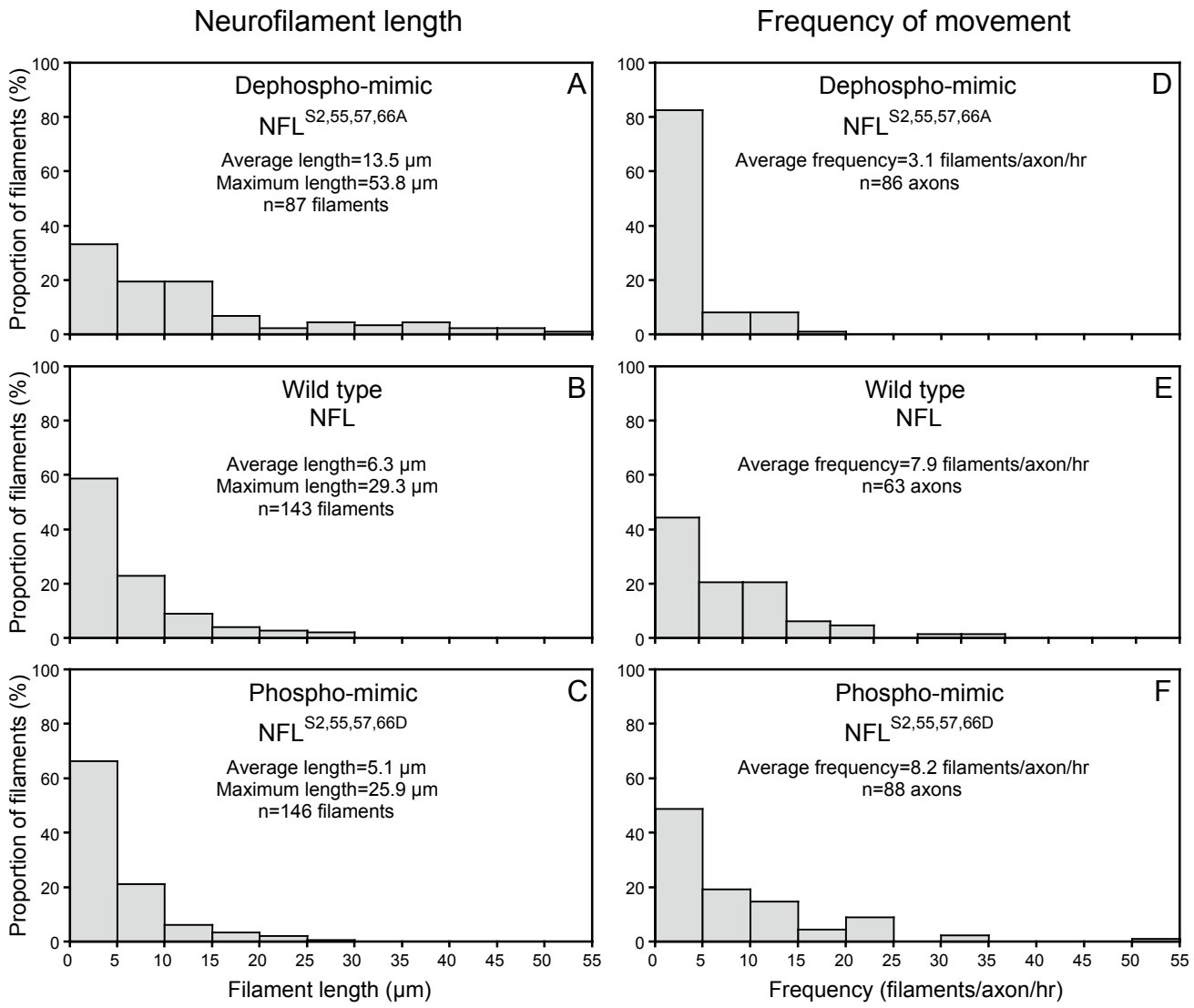
Neurofilament length
Frequency of movement
Dephospho-mimic
NFL S2,55,57,66A
Average length=13.5 μm
Maximum length=53.8 μm
n=87 filaments
A
Dephospho-mimic
NFL S2,55,57,66A
Average frequency=3.1 filaments/axon/hr
n=86 axons
D
Wild type
NFL
Average length=6.3 μm
Maximum length=29.3 μm
n=143 filaments
B
Wild type
NFL
Average frequency=7.9 filaments/axon/hr
n=63 axons
E
Phospho-mimic
NFL S2,55,57,66D
Average length=5.1 μm
Maximum length=25.9 μm
n=146 filaments
C
Phospho-mimic
NFL S2,55,57,66D
Average frequency=8.2 filaments/axon/hr
n=88 axons
F
Proportion of filaments (%)
Filament length (μm)
Frequency (filaments/axon/hr)

Fig. 8

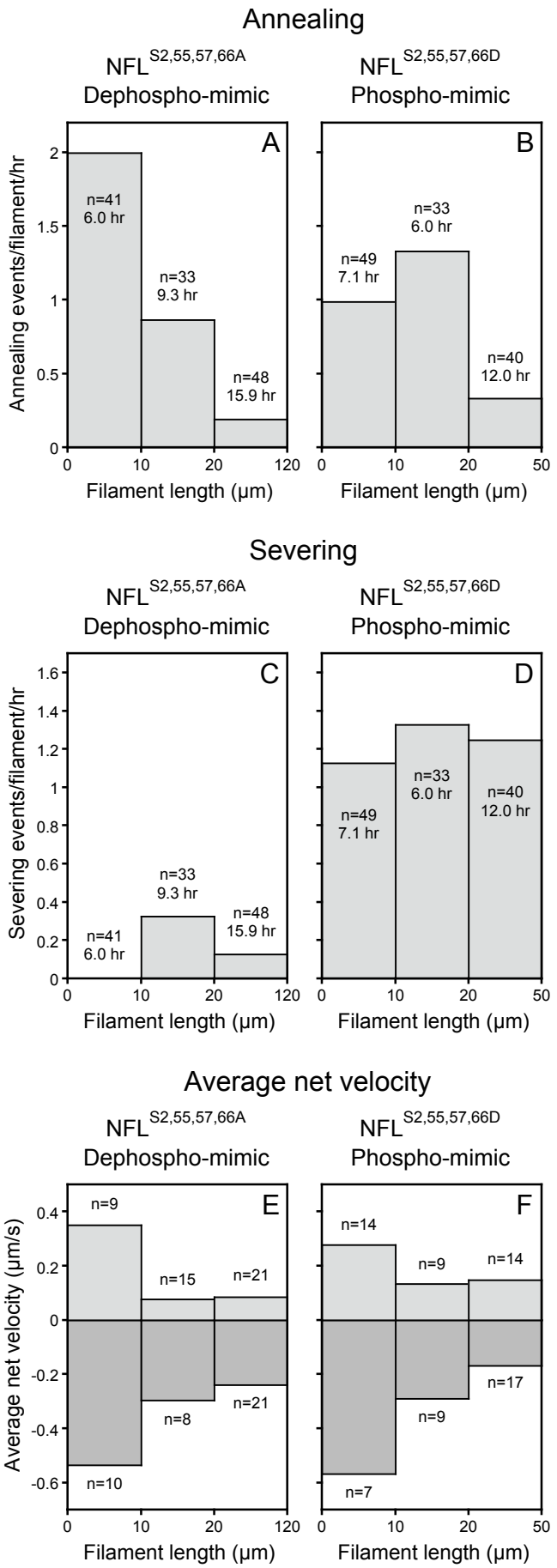
Annealing
NFL S2,55,57,66A
Dephospho-mimic
NFL S2,55,57,66D
Phospho-mimic
A
B
Annealing events/filament/hr
n=41
6.0 hr
n=33
9.3 hr
n=48
15.9 hr
n=49
7.1 hr
n=33
6.0 hr
n=40
12.0 hr
Filament length (μm)
Severing
C
D
Severing events/filament/hr
Average net velocity
E
F
Average net velocity (μm/s)
n=9
n=15
n=21
n=10
n=8
n=21
n=14
n=9
n=14
n=7
n=9
n=17

Fig. 9

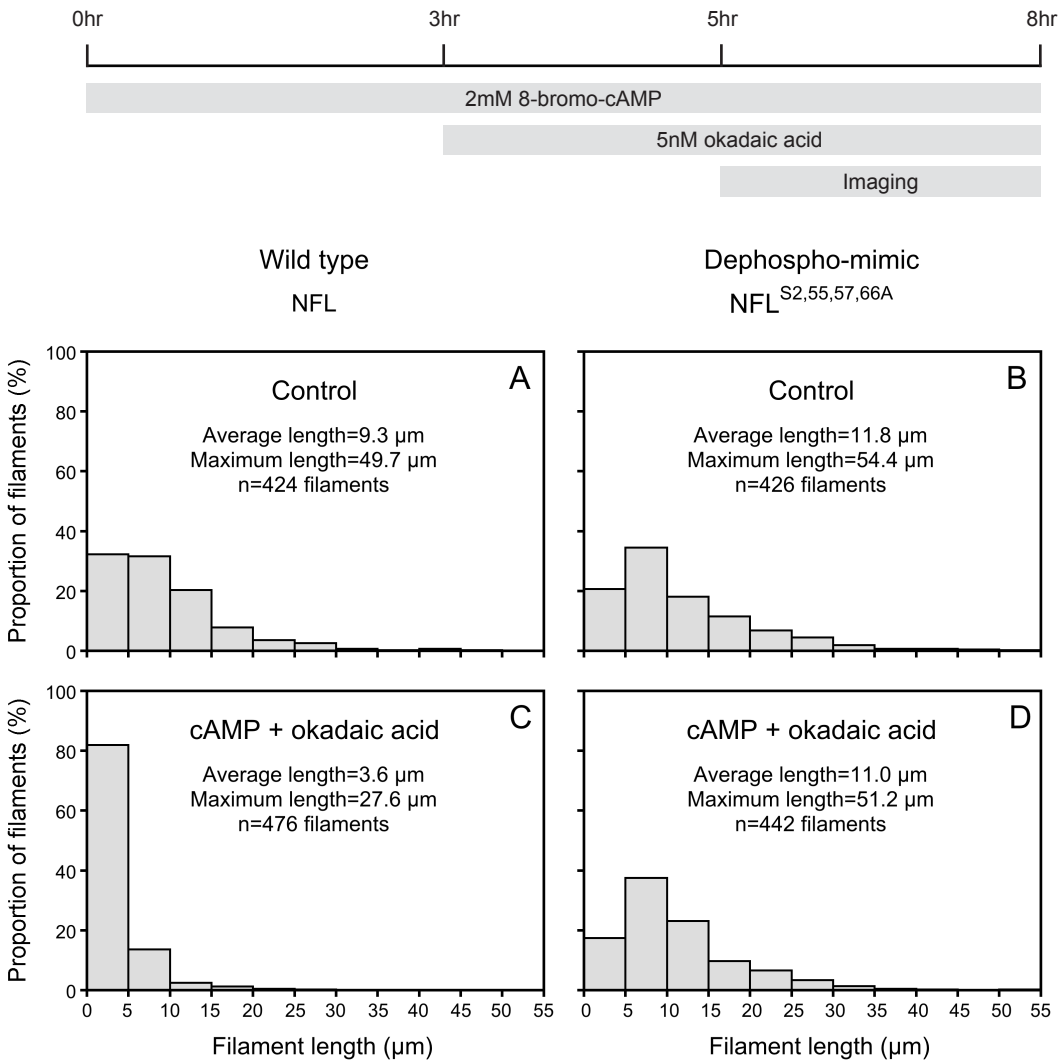
0hr
3hr
5hr
8hr
2mM 8-bromo-cAMP
5nM okadaic acid
Imaging
Wild type
NFL
Dephospho-mimic
NFL S2,55,57,66A
Control
A
Average length=9.3 μm
Maximum length=49.7 μm
n=424 filaments
Control
B
Average length=11.8 μm
Maximum length=54.4 μm
n=426 filaments
cAMP + okadaic acid
C
Average length=3.6 μm
Maximum length=27.6 μm
n=476 filaments
cAMP + okadaic acid
D
Average length=11.0 μm
Maximum length=51.2 μm
n=442 filaments
Proportion of filaments (%)
Filament length (μm)

Fig. 10

A Dynamic cycle of severing and annealing

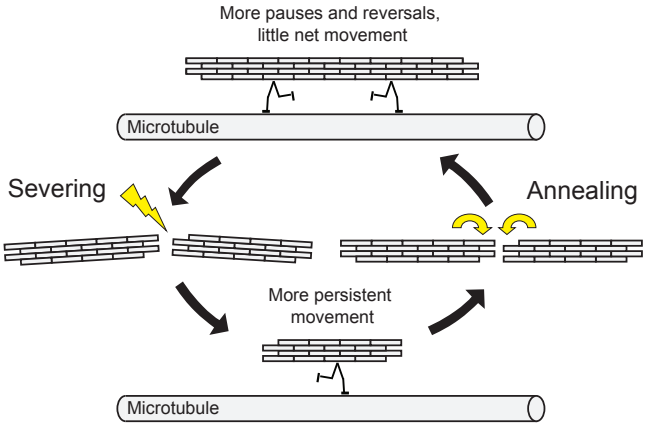
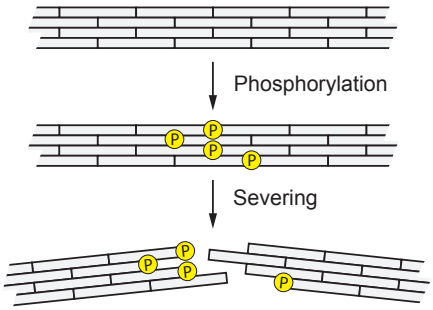
B Proposed severing mechanism